ABSORPTION LINE PROFILES IN A COMPANION SPECTRUM OF A MASS LOSING COOL SUPERGIANT

LILIYA L. RODRIGUES AND ERIKA BÖHM VITENSE[1]

Astronomy Department, FM-20, University of Washington, Seattle, WA 98195

[1] Guest Observer with the International Ultraviolet Explorer which is sponsored and operated jointly by the National Aeronautics and Space Administration, the European Space Agency, and the Science Research Council of the United Kingdom.

ABSTRACT

Cool star winds can best be observed in resonance absorption lines seen in the spectrum of a hot companion, due to the wind passing in front of the blue star.

We calculate absorption line profiles that will be seen in the ultraviolet part of the blue companion spectrum. Line profiles are derived for different radial dependences of the cool star wind and for different orbital phases of the binary.

Bowen and Willson (1986) find theoretically that stellar pulsations drive mass loss. We therefore apply our calculations to the Cepheid binary S Muscae which has a B5V companion.

We find an upper limit for the Cepheid mass loss of $\dot{M} \leq 7 \times 10^{-10} M_{\odot}$ per year provided that the stellar wind of the companion does not influence the Cepheid wind at large distances.

1. INTRODUCTION

1.1. *The Problem*

In their studies of long period variables Bowen and Willson (1986) find large mass loss for these stars due to the pulsation, which expels mass during the expansion phases. Bowen and Willson conclude tentatively that all pulsating stars have strong mass loss and that perhaps all mass loss of luminous stars is due to radial or non-radial pulsations.

For hot stars the mass loss can be best observed in the P Cygni profiles of the UV resonance lines of CIV at 1550$\AA$, SiIV at 1393$\AA$ and 1403$\AA$. For the cool luminous stars mass loss so far has mainly been studied in the CaII K2 emission cores which may show blueshifted absorption components if mass loss occurs. For cool supergiants the MgII resonance lines at 2800$\AA$ may also show absorption components in their emission cores (Stencel et al. 1980) indicative of mass loss. For Cepheids emission cores are rarely seen in these resonance lines and if they show absorption components we cannot be sure whether this means mass loss or whether the structure is due ot the pulsational motions. The observational determination of the mass loss rate is therefore difficult for these pulsating stars.

Another method to determine mass loss of pulsating stars is provided by the observation of Cepheids with hot companions. We can then, in the spectrum of the companion observe the UV resonance absorption lines caused by the Cepheid wind passing in front of the hot companion, see Figure 1. Close to the companion the interaction between a possible wind of the companion and the Cepheid wind may cause some problems for the interpretation, these complications of the line profile occur near zero radial velocity components of the passing wind if observations are

made at the phase shown in Figure 1(a). Large line of sight velocity components of the wind are only seen at large distances from the companion. Wind absorption seen at large blueshifts should not be influenced by the companion wind unless the latter is much stronger than the Cepheid wind. In that case we should see P Cygni line profiles of the companion in the observed spectrum.

In order to determine the mass loss from the Cepheid binary S Muscae we will here calculate the absorption line profiles expected to be seen in the spectrum of the companion S Mus B, which is a B5 main sequence star.

1.2. *Previous Theoretical Studies*

Absorption line profiles expected to be seen in the companion spectrum for hot star/cool supergiant binaries due to the supergiant wind were previously calculated by Hempe (1984) with the α Sco system in mind. He also included the emission by the circumstellar wind material in his line profile calculations. We calculate emission for one set of parameters only and show that for our application it is not important. Hempe considered a velocity law

$$v(r) = v_\infty(1 - R_A/r)^{0.5}, \tag{1}$$

where R_A is the radius of the mass-losing star and v_∞ is the wind velocity at large distances from the star A. Hempe claims that if the turbulent velocity of the wind material is comparable to the wind velocity the exact form of the velocity law does not matter unless the hot companion is 'behind' the cool star. Under most circumstances all velocity laws will produce very similar absorption line profiles.

Our calculations show that this does not hold for velocity laws that decrease with increasing distance from the mass losing star and also velocity laws which give a maximum velocity at some point. While Hempe explores a large range of optical depths along the line of sight and also a large range in $v_\infty/v_{\rm turb}$ we restrict our

calculations to small optical depths and only a few values of $v_{\rm turb}$. (Here, $v_{\rm turb}$ is the turbulent velocity in the wind.) Instead, we concentrate on the changes in absorption line profiles due to different velocity laws.

The organization of this paper is as follows. In Chapter 2 we go over our methods of calculating line profiles. In Chapter 3 we describe the absorption lines calculated for different velocity laws and different orbital phases. We also show the emission line obtained for one special case. In Chapter 4 we discuss the observations for the S Muscae system and compare theoretical and observed line profiles in order to determine the mass loss for S Muscae. Chapter 5 contains a discussion of errors and finally Chapter 6 summarizes our results.

2. METHOD OF CALCULATION

2.1. *The Geometry*

The geometry of the binary system is shown in Figure 1. The coordinate parallel to the line of sight is z, and $z = 0$ in a plane perpendicular to the line of sight that contains the Cepheid. The two stars describe circular orbits around their common center of mass; the distance between the two stars is assumed to be constant. Figure 1 also explains our notation for the orbital phases, ϕ. Angle ϕ is the angle between the line of sight and the line going from the Cepheid to the B star.

It can be seen from Figure 1 that absorption lines sample different columns through the wind at different orbital phases.

For position depicted in Figure 1(a) only material with radial line of sight velocity $v_r \leq 0$ is seen. The wind is sampled for distances r from the cool star for which $r \geq d$ where d is the orbital radius of the blue star around the cool supergiant.

For position in Figure 1(b) the absorption lines sample the wind for distances $r \geq \delta$ where $\delta < d$. Distances $r \leq d$ from the cool star are seen twice: once with the positive and once with negative line of sight velocity component v_r.

In position shown in Figure 1(c), when the hot companion is 'in front' of the cool star, only distances $r > d$ are sampled by the absorption line.

2.2. *Calculations of Absorption Component*

In calculating model line profiles we make some simplifying assumptions about the nature of the wind similar to the ones made by Hempe (1984). Firstly, mass outflow from the mass losing star A is assumed to be spherically symmetric about the center of the star. In a real situation there are a number of factors that can introduce asymmetry into the wind, for example, gravitational perturbation of the mass flow by the hot companion star B, radiation pressure from star B, clumps resulting from instabilities causing small local shocks and turbulence, rotation of the mass losing star, orbital motion of the binary and wind from star B (if present). We do not include these complications. Velocity and density profile as a function of distance from the star are assumed to be constant in time, this means, for instance, that pulsations of the Cepheid are ignored. This may be an unrealistic approximation for this special system since the pulsations may be the very mechanism responsible for driving mass loss. We will come back to this question in Chapter V.

As will be explained later only high velocity components of the wind will be studied in detail and modeled. These wind components arise far from the two stars of the binary and hence we feel justified in assuming that ionization fractions of ions like FeII, SiII, AlIII, etc. remains constant.

The absorption along the column 'in front' of star B (see Fig. 1) is calculated as follows. The column is divided into a large number of segments of length dz. The optical depth $d\tau_\lambda$ is evaluated for each segment, and then contributions due to all line

segments dz are added together to get the total optical depth of the line of sight at one particular wavelength,

$$d\tau_\lambda = n(r) \cdot \kappa_0 \cdot e^{-(\Delta\lambda/\Delta\lambda_D)^2} \cdot dz. \tag{2}$$

Here, r is the distance of the line segment dz from the mass-losing star A, $n(r)$ is the number density of absorbing particles in the line segment dz, and κ_0 is the absorption coefficient per absorbing particle in the center of the line in the rest frame of the absorbers, and

$$\Delta\lambda_D = \lambda_0 \frac{v_{\rm turb}}{c}. \tag{3}$$

Turbulent velocity, $v_{\rm turb}$, is a parameter to be determined by comparison with the observations. The length of each line segment dz was chosen such that the change in the line of sight velocity across dz is very small compared to the turbulent velocity in the wind.

Conservation of mass in the wind requires that

$$4\pi r^2 N(r) v(r) = \text{constant}. \tag{4}$$

For a given $v(r)$ this determines total (i.e., all species) number density $N(r)$. The abundance and the degree of ionization of the line producing element determines $n(r)/N(r)$.

2.3. *Calculation of Emission Component*

The bulk of the emission comes from a large region (linear size of about twice the stellar separation) around the binary. Emission from this circumstellar envelope is dominated by radiative excitations from the light of the B star and deexcitations – collisions can be shown to be unimportant.

We approximate the radiation field of the companion by a Planck function for the $T_{\rm eff}$ of the hot companion B. The number of excitations per unit volume and second

from the ground level at distance r_B from star B is then

$$N_{\rm exc} = J_\nu B_{lu} N_l, \tag{5}$$

where

$$J_\nu = \frac{1}{4} B_\nu(T_{\rm eff}) \frac{{R_B}^2}{{r_B}^2}.$$

B_{lu} is the Einstein B coefficient for stimulated excitation from lower level l to the upper level u. The energy emitted into a unit solid angle in the line is given by

$$\epsilon = N_{\rm exc} h\nu / 4\pi. \tag{6}$$

The wavelength dependence of the emission in the rest frame of the emitting particles is determined by Doppler shifts due to turbulent motions and is given by

$$\varphi(\Delta\lambda) = e^{-(\Delta\lambda/\Delta\lambda_D)^2} / \sqrt{\pi}\Delta\lambda_D, \tag{7}$$

and is centered at $\lambda_r = \lambda_0(1 + \frac{v_r}{c})$, if v_r is the line of sight velocity component of the volume element under consideration.

The energy emitted is reduced due to absorption along the path through the wind. This absorption is calculated in the same way as the absorption in front of star B. Integration of the emission ϵ at each wavelength $\Delta\lambda = \lambda - \lambda_0$ over all volume elements divided by D^2 gives the amount of energy received here per cm^2 per second. D is the distance between the Cepheid and us.

The energy which we receive from star B per cm^2 and second is given by

$$F_\lambda = B_\lambda(T_{\rm eff}) \frac{{R_B}^2}{D^2} e^{-\tau_\lambda}. \tag{8}$$

Both fluxes are proportional to $(R_B/D)^2$. In the normalized profiles these factors cancel.

The emission line profiles calculated here look similar (in general) to Hempe's but are not completely identical to his profiles.

2.4. *Calculation of Mass Loss Rate*

The mass loss rate from the surface of star A is

$$\dot{M} = 4\pi {R_A}^2 \cdot N_0 \cdot v_0 \cdot m_H. \tag{9}$$

v_0 is the wind velocity at the base of star A and m_H is the mass of Hydrogen atom. We assumed that metals do not contribute much to the mass of the outflowing material.

3. ABSORPTION LINE PROFILES FOR DIFFERENT VELOCITY LAWS

3.1. *The Standard Velocity Law*

The velocity law most commonly adopted for luminous OB stars, A-type supergiants (Castor & Lamers 1979), and stars with dense expanding winds, like Of and Wolf-Rayet stars (Olson 1981) is of the form,

$$v(r) = v_\infty(0.01 + 0.99[1 - \frac{R_A}{r}]^\beta). \tag{10}$$

Exponent β is usually assumed to be of the order of 1. Figure 2 shows the radial dependence of the velocity according to equation (10) with $\beta = 0.5$.

The corresponding absorption profiles for phase angles $\phi = 30°, 60°, 90°$ and $150°$ (see Fig. 1) are shown in Figure 3. The scale on the horizontal axis is in terms of the terminal wind velocity, v_∞. Ratio $v_\infty/v_{\rm turb} = 10$. The corresponding mass loss rate if the line is λ2382.03 of FeII is approximately $\dot{M} \approx 1.12 \times 10^{-10} M_\odot.{\rm yr}^{-1}$.

The absorption at the shortest wavelengths corresponding to the largest radial velocities are due to the material at the largest distances from star B. Looking at the absorption line profile in Figure 3 it seems at first sight surprising that the line depth increases for larger radial velocities v_r even though the wind density decreases

for larger radial velocities i.e. larger distances from star A. It can, however, be easily verified that the increase in column length contributing to absorption between v_r and $v_r + dv_r$ more than compensates for the decreasing density.

The sharp dip at the shortest wavelengths is due to material at terminal velocity. Even though the density of absorbers with large v_r, i.e. at large distances from the star is small, the length of the column contributing to absorption is theoretically infinite.

The sharp dip at terminal velocity is common to all the profiles because the absorption at large distances is not affected by the phase ϕ of the system. For phases $\phi \geq 90°$ there is no absorption on the long wavelength side of λ_0 because star B is 'in front' of star A and only the part of the wind which is approaching us is seen in front of B. Phases with small ϕ's (for example, $\phi = 30°$) give rise to deeper absorption profiles than for larger ϕ because at small ϕ our line of sight to star B passes close to star A where the density is high and the wind velocity small. Comparing absorption profiles at ϕ and $180° - \phi$, for example, $\phi = 30°$ and $150°$, one can estimate the amount of absorption in a column between the two positions of star B. This information is useful in mapping out the spatial and velocity structure of the wind.

The ratio of the turbulent velocity to the terminal velocity of the wind has some effect on the shape of the line profile. Turbulence naturally broadens the line, smoothens out sharp edges and spikes. It also moves the position of the lowest flux in the absorption profile (like the one in Fig. 3) to longer wavelengths. This happens because some of the absorbers moving at terminal velocity will be 'redshifted' by large turbulent velocity thus making the number of absorbers at velocities just shy of the terminal velocity large. The solid line in Figure 4 is the same as the $\phi = 90°$ profile of Figure 3. The other two lines of Figure 4 differ from the solid line only in the ratio $v_\infty / v_{\rm turb}$ as shown.

3.2. *Exponential Velocity Law*

In the last section we showed that a monotonically increasing velocity law gives rise to a profile with a broad shallow shoulder and a deep spike-like part on the short wavelength side of λ_0. This spike has an abrupt blue edge. How much and in which way does the absorption line profile change for different velocity laws?

In order to study this we modified the wind velocity law such that after an initially high velocity close to the mass losing star the velocity drops at large distances from the star. This is achieved with an exponential velocity law of the form

$$v(r) = v_0(a \cdot e^{-r/b} + c) \qquad (11)$$

A typical example of such a velocity law is shown in Figure 5, with $a = 30$, $b = 2.5$, $c = 0.12$ and $v_0 = 100$. Note that in this particular case the velocity nearly reaches its asymptotic value at $r/R_A \sim 15$, which is larger than the separation of the stars in the S Mus system.

Since mass flow and radiation field come from two spatially separated sources, the radial velocity distribution, v_r, of the matter in a column in front of star B (i.e., material responsible for absorption) can be quite different from $v(r)$. This point is well illustrated in the present case of an exponentially decreasing velocity law. Figure 6 shows the radial velocity profile along the line of sight as a function of z. There is a hump in v_r, even though $v(r)$ is decreasing monotonically.

Absorption line profiles for this case are shown in Figure 7 for different orbital phases. The velocity is expressed in terms of the terminal velocity, which is $v_0 c$ (see eq. [11]). For small angles ϕ our line of sight to star B passes close to star A where the velocity of outflowing material is large, so the red and blue wings on either side of λ_0 are farther away from the rest wavelength than for larger values of ϕ. Conversely, for ϕ close to 90°, the separation of the two stars on the sky is large. Now light from star B on its way to us passes through slow moving material at large distances from

star A and hence all absorption is very close to λ_0. The central dip which arises due to the material at terminal velocity, is not affected by the phase of the system.

We discuss in detail the absorption line profile generated by this velocity law at orbital phase $\phi = 30°$. The dip just on the short wavelength side of the rest wavelength is due to the wind material at large distances from the star. In addition to this main feature there are also two less prominent features — the shallow broad wings on either side of the line center. The wing at the blueshifted wavelengths comes from material at and near the line of sight velocity peak. Even though the density is quite low there because of the high velocity and large distance from star A, there are two spatially separated regions in the line of sight contributing to the absorption at those v_r's (see Fig. 6). A similar wing appears on the red side — it is due to material from the 'back' side of star A which is streaming away from us.

The main difference of this type of absorption profile compared to that of equation (10) (see Fig. 3) is that the position of the maximum absorption dip is changed. In the case of the standard velocity law most absorption occurs at the shortest wavelengths while in the case of the exponential law it is very close to the rest wavelength. In both cases the amount of absorption at velocities other than terminal velocities varies with the orbital phase of the system.

3.3. *Velocity Laws with a Maximum*

This is a modification of the exponentially declining law considered in the previous section. Equation (11) implies that velocity of the material at the surface of star A is very large. For example, taking equation (11) with $a = 30$, $b = 2.5$, $c = 0.12$ and $v_0 = 100$ gives 2023 km.s^{-1} as the velocity close to the surface of star A, where $r = R_A$. This rather large velocity is very difficult to explain in physical terms since it means that the wind is highly supersonic at the surface of a star. A more physically

plausible situation is achieved by combining equations (10) and (11), namely

$$v(r) = v_0(0.01 + 0.99[1 - \frac{R_A}{r}]) \times (a \cdot e^{-r/R_A b} + c). \qquad (12)$$

It can be easily seen from equation (12) that now the initial velocity is smaller by a factor of 100 (because 1-$\frac{R_A}{r}$ is small there), i.e. $v(R_A)$ is now $\sim$ 20 km.s^{-1} . The velocity then rises rapidly, reaches a peak close to star A (at $r/R_A \sim 2$) and declines exponentially as in equation (11), see Figure 8. The velocity according to equation (10) dominates the one of equation (12) only at small r. The velocity according to equation (12) is therefore similar to the velocity of equation (11) at most radii and therefore the resultant absorption line looks very similar to that obtained with equation (11). (see Fig. 9.) Note, however, that the densities at the surface of the star, and hence the mass loss rates in the two profiles of Figure 9 are very different!

This wind profile is qualitatively similar to the wind profile of some cools stars as given by Carpenter (1984). He deduced the shape of the velocity profile from the FeII asymmetric line profiles in the extended chromosphere of α Orionis. The strongest parts of the line are formed farthest from the photosphere in a decelerating region, intermediate strength line parts are formed in accelerating regions closer to the photosphere and the velocity in the part of the wind closest to the star is almost flat.

4. THE S MUSCAE SYSTEM

4.1. *The Geometry of the S Muscae System*

The physical parameters of the S Muscae system are as follows. S Mus is a binary with an orbital period of 505.2 days and a mass sum of approximately $10M_{\odot}$ (Evans & Bolton 1990). The pulsational period of the Cepheid is 9.66 days (Lloyd Evans 1982). With an observed orbital velocity amplitude $v_r \sin i \approx 13.8$ km.s^{-1} we derive an inclination $i \approx 30°$. Star A, which is a Cepheid, has a radius of roughly $50R_{\odot}$. Radius of star B, a B5V star, is approximately $5R_{\odot}$. Our assumption of a circular orbit for the stars in the binary is justified here since the eccentricity of the S Mus system is, $\varepsilon = 0.03 \pm 0.03$ (Lloyd Evans 1982, Evans & Bolton 1990). The two stars are separated by $\sim 576R_{\odot}$. The effective temperature of star B was taken to be $17,000°$K (Böhm-Vitense & Proffitt 1985), and its spectrum in the UV region was approximated by a black body at that temperature.

The geometry of the system and the direction to the observer at different orbital phases are shown in Figure 1. As was explained in Chapter 2, at different orbital phases the line of sight to the hot companion may pass through the wind at different distances from the mass losing star.

In addition to determining the wind velocities at different distances r from the cool star we can also sample the degree of ionization of the wind at different distances from the star by observing the line profiles for lines of different ions. Such studies are only possible in the ultraviolet where strong resonance lines of FeI, FeII, MnII, SiI, SiII, SiIII, SiIV, CII, CIV, AlI and AlIII can be observed in the spectrum of the B5 star unimpeded by the varying Cepheid lines. Note that the degree of ionization of the cool star wind may be expected to be higher close to the blue companion either due to a shock developing around the B star if it accretes material or, if the B star is losing mass, due to the shock in the region where the winds from both stars collide.

(See Che-Bohnenstengel & Reimers 1986.)

4.2. *The Ultraviolet Spectra of S Muscae*

The observational data used in this paper was taken by the IUE satellite in the period 1982-1988 using LWR, LWP and SWP cameras. Most of the observations were done by one of us (E. B.-V.). The complete list of the spectra, the dates they were obtained, the orbital phase of the S Mus binary system and the pulsational phase of the Cepheid at those times are given in Table 1. Most of the spectra were taken at the maximum radial velocity phase, i.e. orbital phases 0.25 and 0.75.

Figures 10, 11, and 12 show spectra of several ions at various orbital phases of the system (see Table 1). (Note: only standard IUE processing was used to obtain these spectra.) All spectra in Fig. 10 and 11 were taken at an orbital phase $\phi = 90°$. The line profiles for $\lambda < 2400\AA$ are very noisy because of the low sensitivity of the camera for these wavelengths. All the resonance lines have a very deep absorption feature close to the 0 radial velocity. This central feature does not vary with the phase of the system and ~~is believed to be~~ probably has a large interstellar contribution mostly due to the interstellar material. The equivalent widths of these central lines are somewhat larger than what would be expected given the reddening of S Mus. The widths of these lines ($\frac{1}{2}$FWHM $\sim$ 28 km.s^{-1}) are slightly higher than the typical velocity dispersions of interstellar clouds indicating contribution from other sources. If part of the central feature is due to the wind of star B then that could in principle account for the width of the line and also the fact that $\phi = 90°$ lines are slightly redshifted from 0 km.s^{-1} .

At orbital phase $\phi = 90°$ most of the 0-volt resonance lines of FeII (Fig. 10), SiII, AlIII with moderately good signal to noise ratio, have a gentle extended dip at about -170 km.s^{-1} from the line center. We need a theoretical profile that reproduces this blue dip at $\phi = 90°$ and possibly shows some absorption close to the rest wavelength.

The extended blueshifted dip is absent in some other resonance lines, most notably

in the weaker MnII lines (Fig. 11, 12). The absence of this feature in non-resonance lines can be explained by the lower abundance of Mn as compared to Fe, about a factor of 100.

There is another absorption feature which is common to many lines. The short wavelength side of the central absorption dip has a gentler slope than its long wavelength counterpart. This feature is quite prominent in the lines of FeII, MnII, SiIV, AlIII at *all* orbital phases of the system (Fig. 10, 11, and 12) though it appears to be variable.

This feature shows low line of sight velocity components and therefore could possibly be an interstellar component. In order to check this we looked at the spectrum of a B2V star in a different direction of the sky, HD 3369, and found similar line profiles for several lines. This suggests that this extended blue wing is probably intrinsic to the star. The apparent variability of the feature argues against an interstellar origin.

This feature might then be due to a B star wind. The appearance of this extended wing also in the supposedly single star HD 3369 would argue in favor of this interpretation. We checked the line profile which would be expected for a single B star wind assuming the velocity law for this wind to be of the form given in equation (10). Figure 13 shows the expected line profile, which looks rather similar to the observed one. (Note, however, that in this case the total number density at the surface of the single star has been reduced by a factor of 10 to make the profiles look similar.) It surprises us, however, that the wind of a star with 17,000K should have such a low degree of ionization. We do however also see some indication of a 'blue' wing in some higher ionization particles like CIV.

It may also be possible that this feature could be due to the Cepheid wind close to the B star. In any case the interpretation of this feature is ambiguous. We therefore concentrate on the shorter wavelength absorption components which originate

in material with a large line of sight velocity which means material which is at large distances from star B. This material is not disturbed by the B star wind and gives us more reliable information about the Cepheid wind. (If the B star wind carries a larger momentum than the Cepheid wind it could blow away the Cepheid wind, we would then see a typical stellar wind line profile for the B star lines, which we do not observe.)

4.3. *Fitting Model Line Profiles To Observations*

We have the best spectra and also most spectra for phase $\phi = 90°$. We shall therefore use these spectra. The shallow dip on the blue side of the rest wavelength can be well approximated by the monotonically increasing velocity law given by equation (10). The other two velocity laws would yield extended dips ('satellite' features) only at phases other than $\phi = 90°$. (See Fig. 7, 9.) Therefore we are going to assume the velocity law of equation (10) with $\beta = 0.5$ in all our subsequent profile comparisons.

Theoretical profiles based on this velocity law and the geometry of the S Muscae system were fitted to several FeII, MnII and AlIII lines. (Fig. 14) Note that it is only the shallow blue wing around -170 km.s^{-1} that is being modeled here. The central feature (close to 0 km.s^{-1}) is probably mostly interstellar as discussed earlier. Using solar abundances of elements, i.e. Fe/H=3×10^{-5}, Mn/H=2.5×10^{-7}, Al/H=2×10^{-6}, the set of parameters that fit the observed profiles best are as follows (solid line): v_∞ = 220 km.s^{-1} , $v_{\rm turb}$ = 50 km.s^{-1} , and the mass loss rate, $\dot{M} = 1.5 \times 10^{-10} M_\odot {\rm yr}^{-1}$ assuming that Fe is all in the form of FeII. Since the 'dips' differ a little from line to line and from spectrum to spectrum due to mainly noise, there is a range of parameters that can fit the observed line profiles equally well. For example, the following set of parameters will also fit the profiles (dashed line in Fig. 14) v_∞ = 185 km.s^{-1} , $v_{\rm turb}$ = 37 km.s^{-1} , and $\dot{M} = 1.13 \times 10^{-10} M_\odot {\rm yr}^{-1}$. (Note that lines whose spectra do not show any blue wing absorption (e.g. AlIII λ1854.72, AlIII λ1862.78

and MnII λ2605.70) are not expected to have any observable absorption according to the model.) The mass loss rates in both cases are very similar. The mass loss rate is thus smaller than might have been expected for a pulsating star if mass loss is indeed mainly occuring due to pulsations. Could the emission from the envelope influence the result? We have calculated the emission from the envelope around the binary using the second set of parameters above. Figure 15 shows a 2382$\AA$ resonance line of FeII with four theoretical lines superimposed on it. A pure absorption line and a final line profile including emission. The two types of line, solid and dashed, have the same meaning as in Figure 14. A slight improvement in the fit may perhaps be seen when including the weak emission. The emission part of the line profile is not, however, important in comparison with the absorption for the following reasons: firstly, the strength of the emission was always found to be much less than the corresponding absorption, and secondly, since the bulk of the emission comes from the region between the two stars where both the density of the wind material and the radiation intensity are high, the emission is usually not far displaced from the line center where it is almost completely covered up by much stronger interstellar absorption. Because of these factors we have concentrated on the far wings of the absorption corresponding to high radial velocities.

5. ERROR DISCUSSION

Several sources of error have to be considered.

5.1. *Placement of the Continuum*

Since the short wavelength absorption wing is wide and shallow and since the spectra are noisy we may misjudge the position of the continuum. Because these wings are optically thin the derived mass loss rate is directly proportional to the

depth. The true line depth would have to be twice as deep as adopted for the mass loss rate to be twice the derived value. This seems to be an upper limit for the uncertainty in the line depth. An error of this kind will not change the order of magnitude for the mass loss rate.

Any error in the adopted oscillator strength would also be of minor importance.

5.2. *Degree of Ionization of the Wind*

In deriving the mass loss rate we assumed that iron is all in the form of FeII. There are no usable FeIII lines in the IUE wavelength region. We therefore looked at the AlIII resonance lines at 1854.7$\AA$ and 1862.8$\AA$ to see whether any blue wings due to mass loss could be seen. Figure 14 shows the observed line profiles. We see no indication of blue wings. AlII has an ionization energy of 18.82eV while FeII has an ionization energy of 16.18eV. The difference is very small. The abundance of Al is a factor of 10 less than Fe. The oscillator strengths of the AlIII lines are a factor of 2.6 larger than the one for the 2599.4$\AA$ line (f=0.565 for the AlIII 1854.7$\AA$ line and f=0.22 for the FeII 2599.4$\AA$ line). If there would be 5 times as much AlIII as AlII we should see the shallow blue wing of AlIII line as strong as the FeII line. Since we do not see any AlIII we conclude that there could be at most 3 times as much FeIII as FeII if any at all.

We thus conclude that the derived mass loss rate due to these effects could be wrong by at most a factor of 6, if both the uncertainties conspire to work in the same way.

5.3. *Reality of Blue Wing*

We might ask whether the shallow dip around -170 km.s^{-1} is actually due to the wind of the companion. Could it be intrinsic to the B5V star spectrum? The profile does not support this suspicion, however we did look at the UV spectra of HD 60098,

a standard single B4V star. Some lines in its spectra seemed to have a shallow dip at around -170 km.s^{-1} . There are very few good IUE comparison spectra for standard stars of this spectral type. Most of the observed stars are either peculiar or have high rotational velocities. In any case assuming that the shallow dip is due to the Cepheid wind gives us an upper limit for the Cepheid mass loss. We then conclude that for the S Mus Cepheid, $\dot{M} \leq 7 \times 10^{-10} M_{\odot}$ per year.

5.4. *Periodic Variations*

Could it be that the wind of the Cepheid varies periodically and we just happened to study the wind absorption at a phase when little material is passing by the B5V star? For the phase $\phi = 90^{\circ}$ we have observations for a whole pulsational cycle (Böhm-Vitense et al. 1990). We do not see any systematic variations for this time interval. Should we expect any variations at all?

If we assume that the Cepheid mass loss occurs in discrete bursts then we might be able to see these in the absorption line. Along the line of sight we should see density enhancements at certain intervals. These high density regions would correspond to different line of sight velocity components. We might then see increased absorptions at regular intervals. We find, however, that the line of sight velocity separations of these high density regions are typically smaller than the turbulent velocity in the wind. Hence any discreteness in the wind that might have been there to start with will be washed out by the turbulence in the wind. So we do not expect to see variations in the shape of the absorption line during the course of a pulsational cycle.

5.5. *Disturbance of the Cepheid Wind by a Possible Wind of the B5V Companion*

Little is known about winds from B5V stars, but they are assumed to be weak and the corresponding mass loss small. (Note, however, that Hagen, Hempe and Reimers (1987) claim to see a wind from α Sco companion (B4V) with about 500 km.s^{-1} in

the SiII lines, which is however not seen in the FeII, CrII or NiII lines.)

If a B5V stellar wind is present its mass loss line profile should not vary in any systematic way for different orbital phases while the Cepheid wind profile should vary systematically in the manner described above. The two stellar winds should thus be distinguishable.

For the S Mus companion we do sometimes see an extended wing in the SiIV 1393$\AA$ line, but it is not seen in the weaker 1402$\AA$ line. It is therefore likely that the wing in the 1393$\AA$ line is due to another line. We may see an asymmetry in the AlIII 1854.7$\AA$ line and in the FeII line at 2585.9$\AA$ (Fig. 14) which may be due to a B5V star breeze.

The asymmetry in the line extends to $v_r \sim -50$ km.s^{-1} . For a B5V star the escape velocity is $\sim$700 km.s^{-1} . It is therefore doubtful whether the asymmetry is indeed due to a wind which escapes from the star. If it is due to an escaping wind then the high velocity densities are so small that we do not see most of the wind absorption line, we only see the part of the line at small velocities, $v_r > -50$ km.s^{-1} , i.e. close to the B star. This means that at velocities $v_r \sim$100 km.s^{-1} which we study $(\rho \cdot v)$ from the B5V star must be less than $(\rho \cdot v)$ from the Cepheid, where ρ and v are density and velocity of the wind respectively. The momentum from the B star wind is therefore smaller than the one from the Cepheid. We therefore do not think that it is possible for the B5V star wind to "blow" the Cepheid wind out of the line of sight column.

6. CONCLUSIONS

In this paper we have considered three different types of velocity laws for mass loss from stars. The three types are: a monotonically increasing law, a monotoni-

cally decreasing law (exponential decline), and a combination of both, a wind which accelerates, reaches a peak and decelerates to a constant terminal velocity.

The corresponding absorption lines arising in the spectrum of the companion were calculated for different parameters of the velocity law and different orbital phases of the binary system. The material responsible for absorption on the one side and the radiation field on the other side were assumed to come from two spatially separated sources, star A and star B respectively. This special geometry gave rise to interesting absorption line shapes.

For monotonically increasing wind velocities we find the deepest absorption at the short wavelength edge of the absorption line at the terminal velocity.

For outward decreasing wind velocities the radial velocity along the line of sight shows maxima leading to more or less broad and flat 'satellite' components whose wavelengths depend on both, orbital phase and the velocity law. Observing the absorption lines at different phases permits the separation of the phase effects and the wind velocity law.

The analysis of the spectra of S Mus system is complicated by a number of factors: firstly, part of the observed absorption features in the SWP spectra are due to interstellar material, and part could be due to the wind of the hot companion. In the LWR spectra the eclipsed lines also contribute. Secondly, the gravity field of star B could, in principle, influence the pattern of the wind material velocity, such that part of the material close to the B star might be falling towards star B. In this case we should have some absorption on the long wavelength side. There is some indication of that in the spectra of some lines but the evidence is insufficient. Thirdly, most of the spectra are plagued with irregular bumps and dips, some of which are, of course, noise, but some could be due to the non-uniform nature of the wind. For example, turbulence in the wind can produce local shocks which will lead to a distorted line profile shape. By observing only the parts of the wing for $v_r < -50$ km.s^{-1} we avoid

problems with material close to the B5 companion. This also avoids the problems with the interstellar lines.

In order to deal with the above difficulties we have to make some simplifying assumptions about the S Mus system and then proceed with the fitting. We assume a spherically symmetry wind which should be a good approximation for the large distances from the B5 star which we are studying. The velocity law that fits the observations best is given by equation (10). The corresponding mass loss is derived to be of the order of $10^{-9} - 10^{-10} M_{\odot} \mathrm{yr}^{-1}$. This would be an upper limit if the shallow blue wing dip were not entirely due to the Cepheid wind. Considering uncertainties in the continuum fitting and in the degree of ionization the mass loss could possibly be larger by a factor of 6.

We do not think that a possible wind from B5V star companion could disturb the Cepheid wind enough to have an effect on our mass loss determination.

The main conclusion of this study is then that whatever the exact form of the velocity law is and whether or not star B has a wind of its own, the mass loss rate from the Cepheid is very small, $< 7 \times 10^{-10} M_{\odot} \mathrm{yr}^{-1}$. A more comprehensive study is necessary to determine whether mass loss from other, especially longer period Cepheids may be larger. A search for long period Cepheids with suitable blue companions is necessary to make such a study possible.

Acknowledgements

This research was made possible by NASA grant NSG 5398, which is gratefully acknowledged.

We are also very much indebted to the staff of the IUE observatory without whose help and support the observations underlying this research would not have been possible.

TABLE 1

Observational Data

Spectrum	Date	Orbital Phase	Pulsational Phase
LWP 3035	1984, 78 day	0.29	0.030
LWR 13849	1982, 215 day	0.10	0.700
LWR 15538	1883, 81 day	0.56	0.625
LWR 15975	1983, 139 day	0.67	0.643
SWP 31542	1987, 224 day	0.72	0.739
SWP 31543	1987, 224 day	0.72	0.739
SWP 33435	1988, 124 day	0.25	0.125
LWP 13163	1988, 124 day	0.25	0.125
LWP 13176	1988, 128 day	0.25	0.562
LWP 13183	1988, 129 day	0.25	0.643
LWP 13196	1988, 131 day	0.25	0.944
LWP 13233	1988, 136 day	0.25	0.436

REFERENCES

Böhm-Vitense, E., Cottrell, P., Clark, Wallerstein, G. 1990, AJ, 99, 353.

Böhm-Vitense, E., Proffitt, C. 1985, ApJ, 296, 175.

Bowen, G. H., Willson, L. A. 1986, Ir. AJ, 17, 249.

Carpenter, K. G. 1984, ApJ, 285, 181.

Che-Bohnenstengel, A., Reimers, D. 1986, A&A, 156, 172.

Evans, N. R., Bolton, C. T. 1990, ApJ, 356, 630.

Hagen, H.-J., Hempe, K., Reimers, D. 1987, AJ, 184, 256.

Hempe, K. 1983, A&A Suppl., 53, 339.

Hempe, K. 1984, A&A Suppl., 56, 115.

Lloyd, Evans, T. 1982, MNRAS, 119, 925.

Olson, G. L. 1981, ApJ, 245, 1054.

Stencel, R. E., Mullan, D. J., Linsky, J. L., Basri, G. S. and Worden, S.P. 1980, ApJS, 44, 383.

Figure Captions

Fig. 1.—The geometry of the binary system at various phase angles, ϕ. A is the mass losing star, and B is the blue companion. The shaded column shows the material seen in absorption by the observer. (a) ϕ=90°, (b) ϕ <90°, (c) ϕ >90°.

Fig. 2.—Standard velocity law as a function of the distance from the mass losing star A. The form of the velocity law is $v(r) = (0.01 + 0.99[1 - R_A/r]^{0.5})$.

Fig. 3.—Absorption line profiles from a binary system. The velocity law is shown in Fig. 2. Different line types correspond to different phase angles of the system: ϕ=30°, 60°, 90°, and 150°. The ratio of the terminal wind velocity to the turbulent velocity in the wind, $v_\infty/v_{\rm turb}$, is equal to 10 for all four profiles.

Fig. 4.—Absorption line profiles for the velocity law shown in Fig. 3. The three different types of lines correspond to three ratios of the terminal velocity of the wind to its turbulent velocity: $v_\infty/v_{\rm turb}$=3, 10, and 15.

Fig. 5.—Exponential velocity law as a function of the distance from the mass losing star. The form of the velocity law is $v(r) = v_0(30e^{-r/2.5R_A} + 0.12)$ km.s^{-1}.

Fig. 6.—Radial profile, v_r, of the exponential velocity law shown in Fig. 5 as a function of the radial coordinate, z. The phase of the binary is ϕ=90°. Notice that the profile is not a monotonous function; in particular, it exhibits a peak at a distance of $5R_A$ from the blue companion.

Fig. 7.—Absorption line profiles at different orbital phases of the binary, ϕ=30°, 40°, 60°, 90°, and 150°. Velocity law shown in Fig. 5 was used. The ratio $v_\infty/v_{\rm turb}$ is 10 for all five profiles.

Fig. 8.—A velocity law with a maximum as a function of the distance from the mass losing star, $v(r) = v_0(0.01 + 0.99[1 - R_A/r]) \cdot (30e^{-r/2.5R_A} + 0.12)$ km.s^{-1}. Notice that the velocity profile has a peak at a distance smaller than the separation of the two stars in the binary.

Fig. 9.—A comparison of absorption lines profiles for two different velocity laws: the solid line corresponds to velocity law of Fig. 5, the dashed line corresponds to that of Fig. 8. The orbital phase ϕ is 30° in both cases. Notice that even though the shapes of the two line profiles are similar in both cases, the number of absorbers along the line of sight is not. Mass loss rate for the dashed line profile (velocity law with a maximum) is 2.5×10^5 times larger than the one for the solid line profile (exponential velocity law).

Fig. 10.—Observed line profiles of five resonant FeII lines. All spectra were taken at an orbital phase ϕ=90°.

Fig. 11.—Observed line profiles of four resonant MnII lines. All spectra were taken at an orbital phase ϕ=90°. Note that four features in this Figure are crossed out and labeled *R*. These are reseau marks.

Fig. 12.—Observed line profiles of resonant lines of MnII. These spectra were taken at orbital phases other than ϕ=90°.

Fig. 13.—Absorption line profiles of the velocity law given in Fig. 2. The solid line shows the profile that would arise from a single star. The dashed line corresponds to a line seen in a binary, where mass outflowing from one star is illuminated by light from the hot companion star.

Fig. 14.—Six panels show observed line profiles of several resonant lines and two model fits to each line. Note that it is the shallow wing at around -170 km/s that is being fit, not the central part of the line! Both models assume the standard form of the velocity law shown in Fig. 2. The parameters of the velocity law are as follows: solid line, v_∞ = 220 km.s^{-1}, $v_{\rm turb}$=50 km.s^{-1}, and the mass loss rate, $\dot{M}$ = $1.5\times10^{-10}M_\odot$ yr^{-1}; dashed line, v_∞=185 km.s^{-1}, $v_{\rm turb}$=37 km.s^{-1}, and $\dot{M}$ = $1.13\times10^{-10}M_\odot$ yr^{-1}. Note that we did not attempt to model the central strong component of the absorption line because it is probably mostly interstellar.

Fig. 15.—The influence of the emission part of the line on the line profile as a whole. A resonant line of FeII is used as an example. One set of solid and dashed lines represents absorption only, while the other set of lines corresponds to the absorption plus emission. It can be seen that emission introduces very little difference into the line profiles far from the rest wavelength. (Note that it

is only the shallow blue wing that is being fit.)

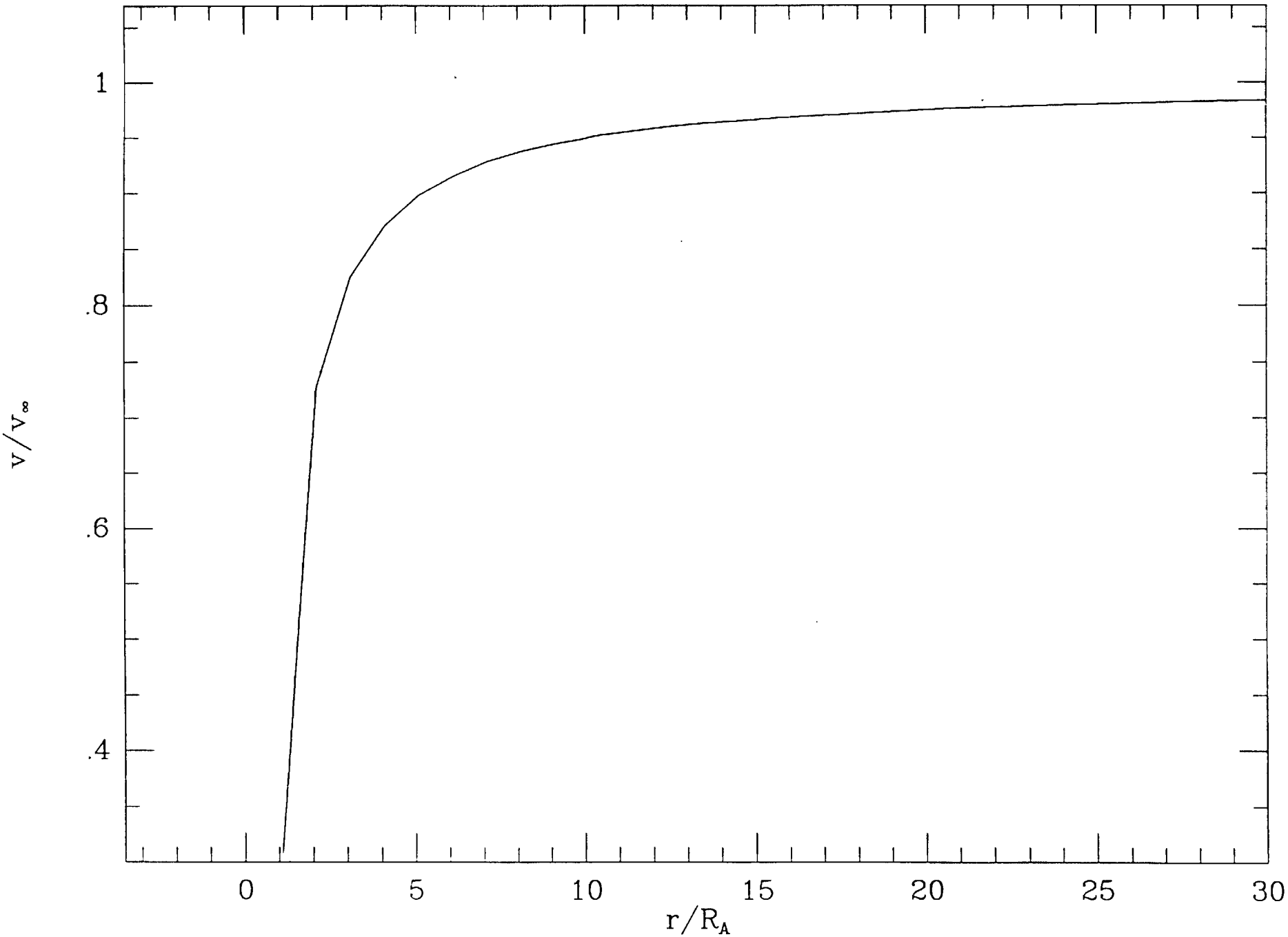
1
.8
.6
.4
v/v∞
0
5
10
15
20
25
30
r/R_A

(a)

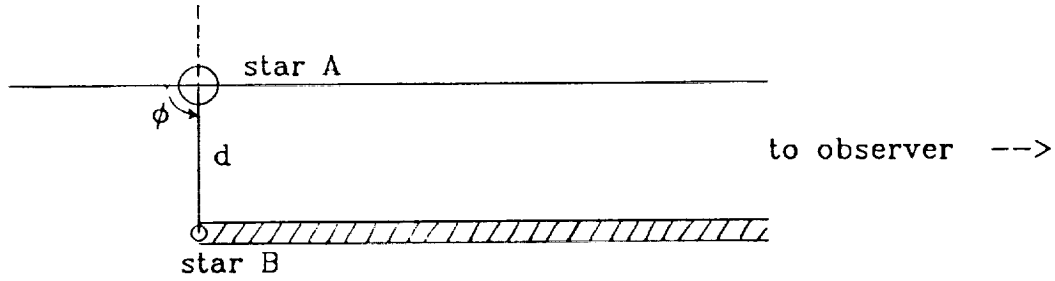
star A
ϕ
d
to observer -->
star B

(b)

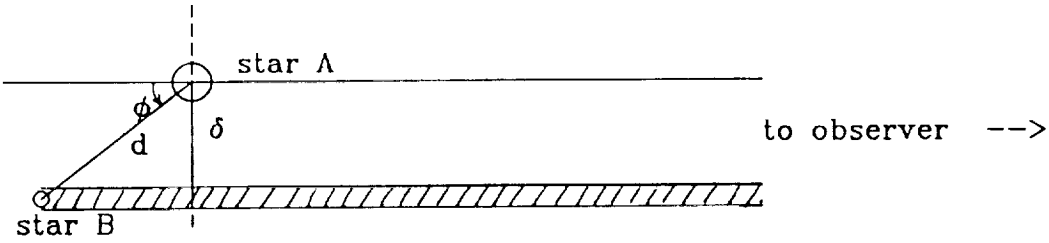
star A
ϕ
d
δ
to observer -->
star B

(c)

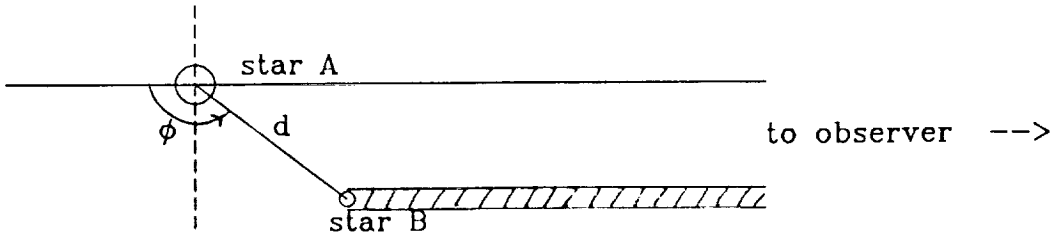
star A
ϕ
d
to observer -->
star B

Fig. 1

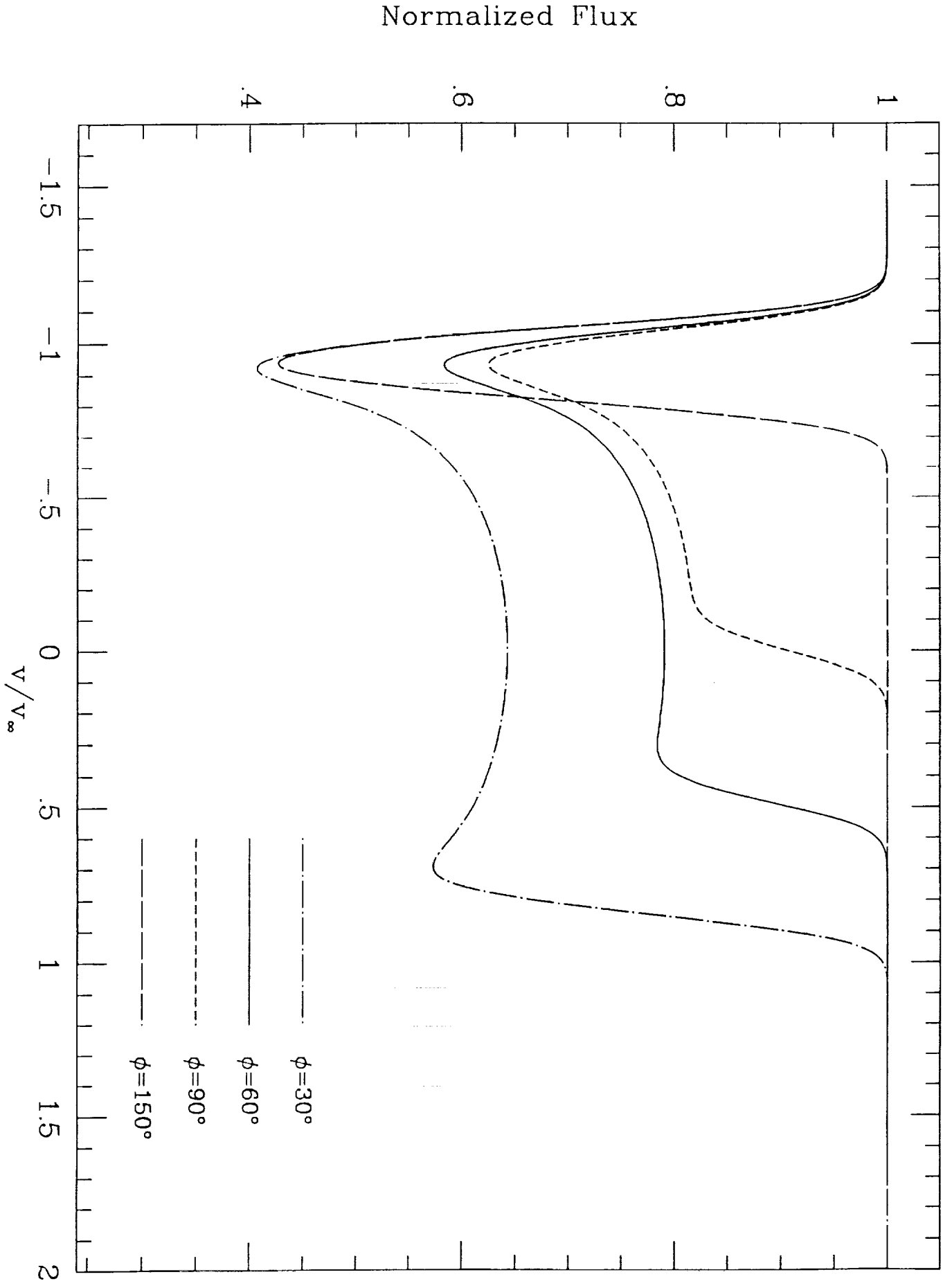
Normalized Flux
1
.8
.6
.4
-1.5
-1
-.5
0
.5
1
1.5
2
v/v∞
φ=30°
φ=60°
φ=90°
φ=150°

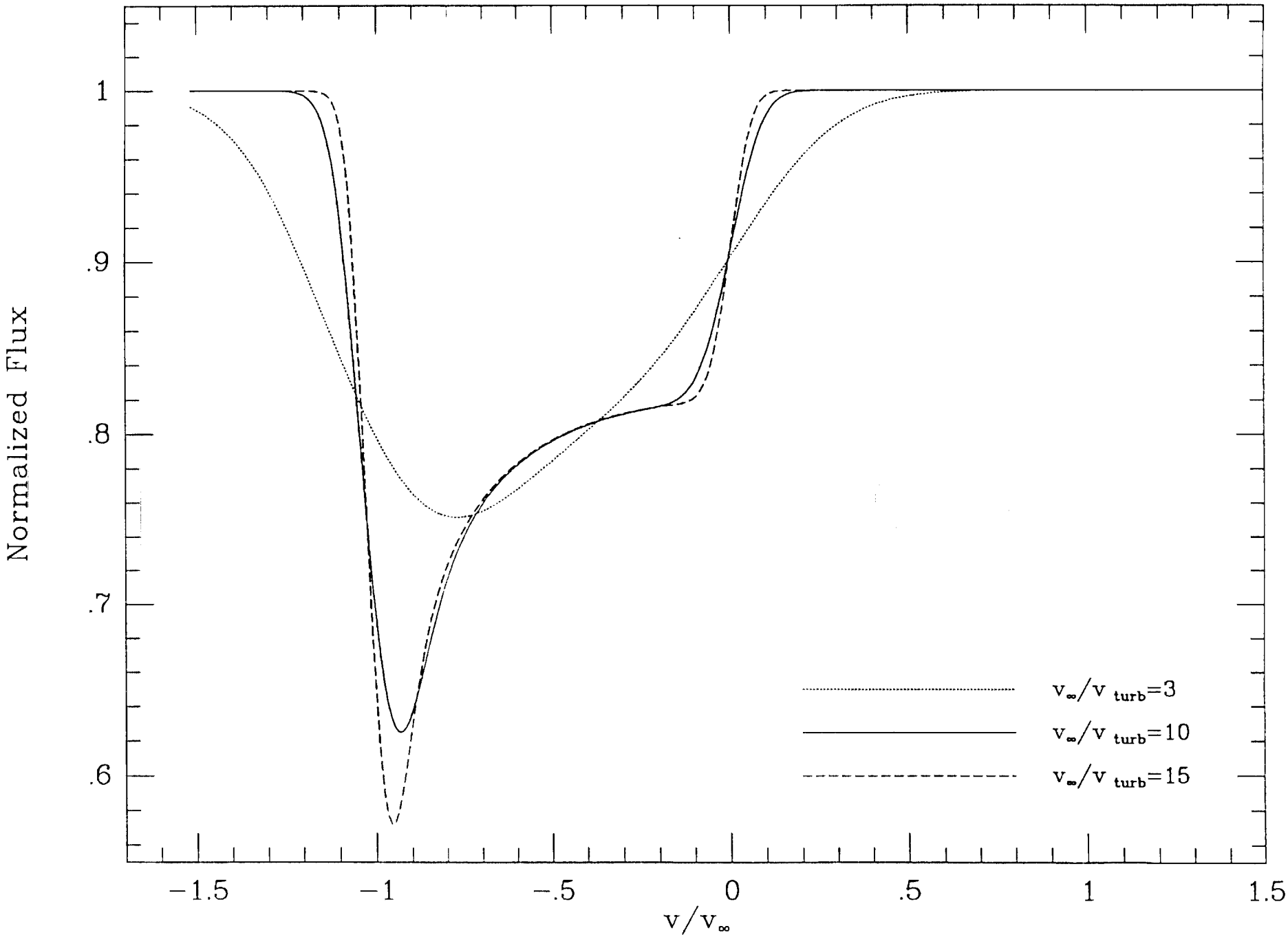
Normalized Flux
1
.9
.8
.7
.6
−1.5
−1
−.5
0
.5
1
1.5
v/v∞
v∞/v turb=3
v∞/v turb=10
v∞/v turb=15

Fig 4

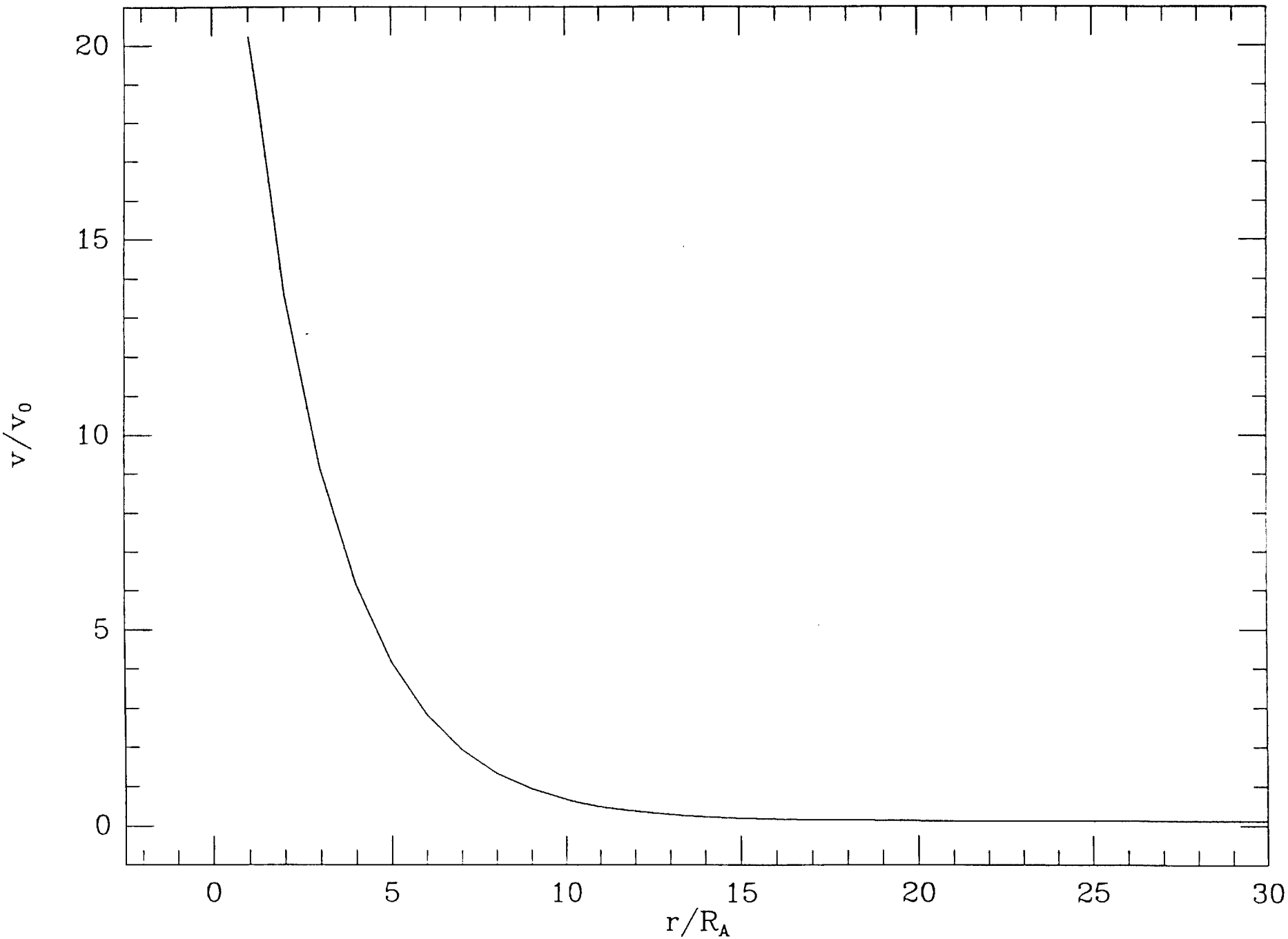
20
15
10
5
0
v/v0
0
5
10
15
20
25
30
r/RA

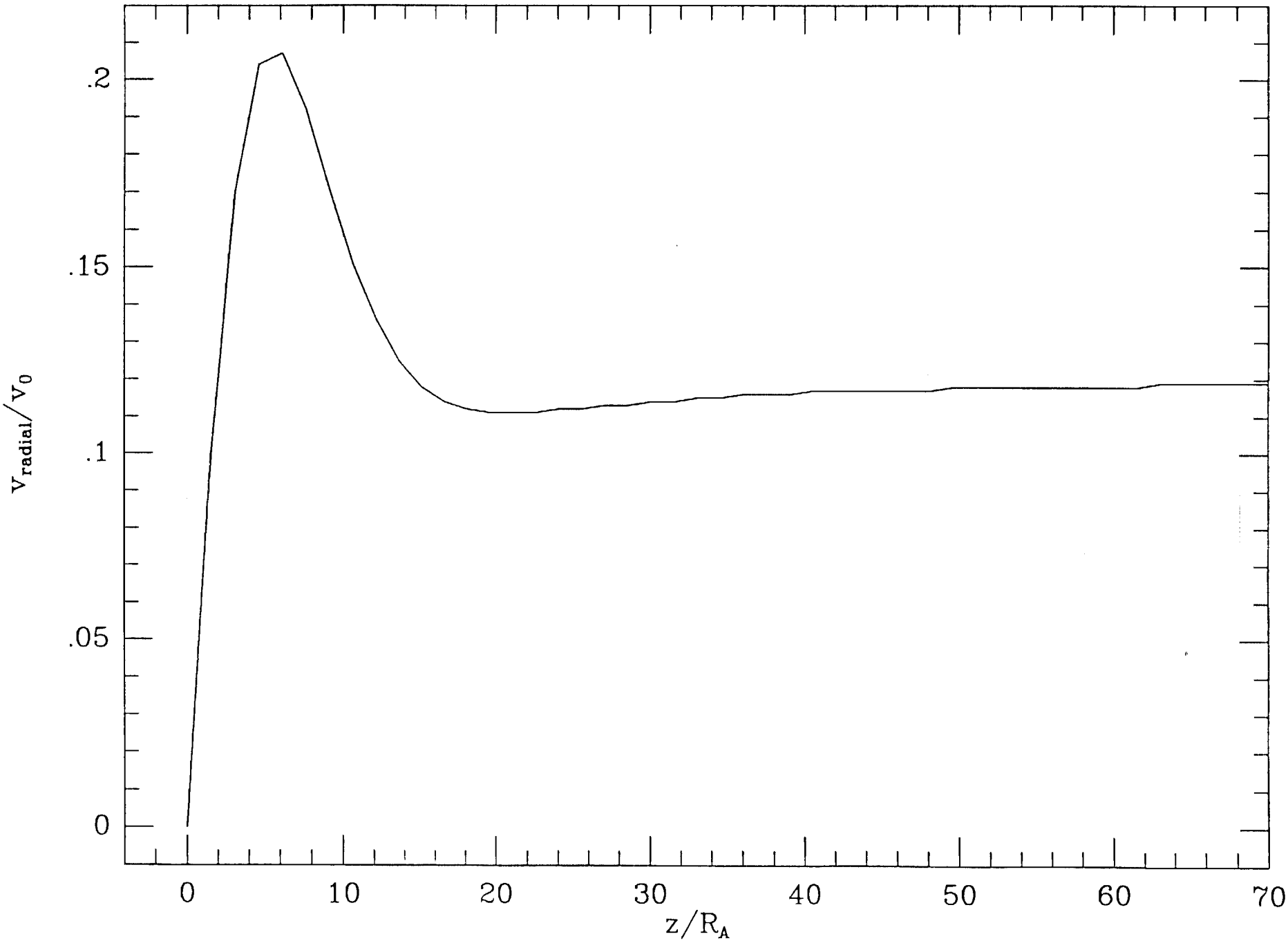
.2
.15
.1
.05
0
v_{radial}/v_0
0
10
20
30
40
50
60
70
z/R_A

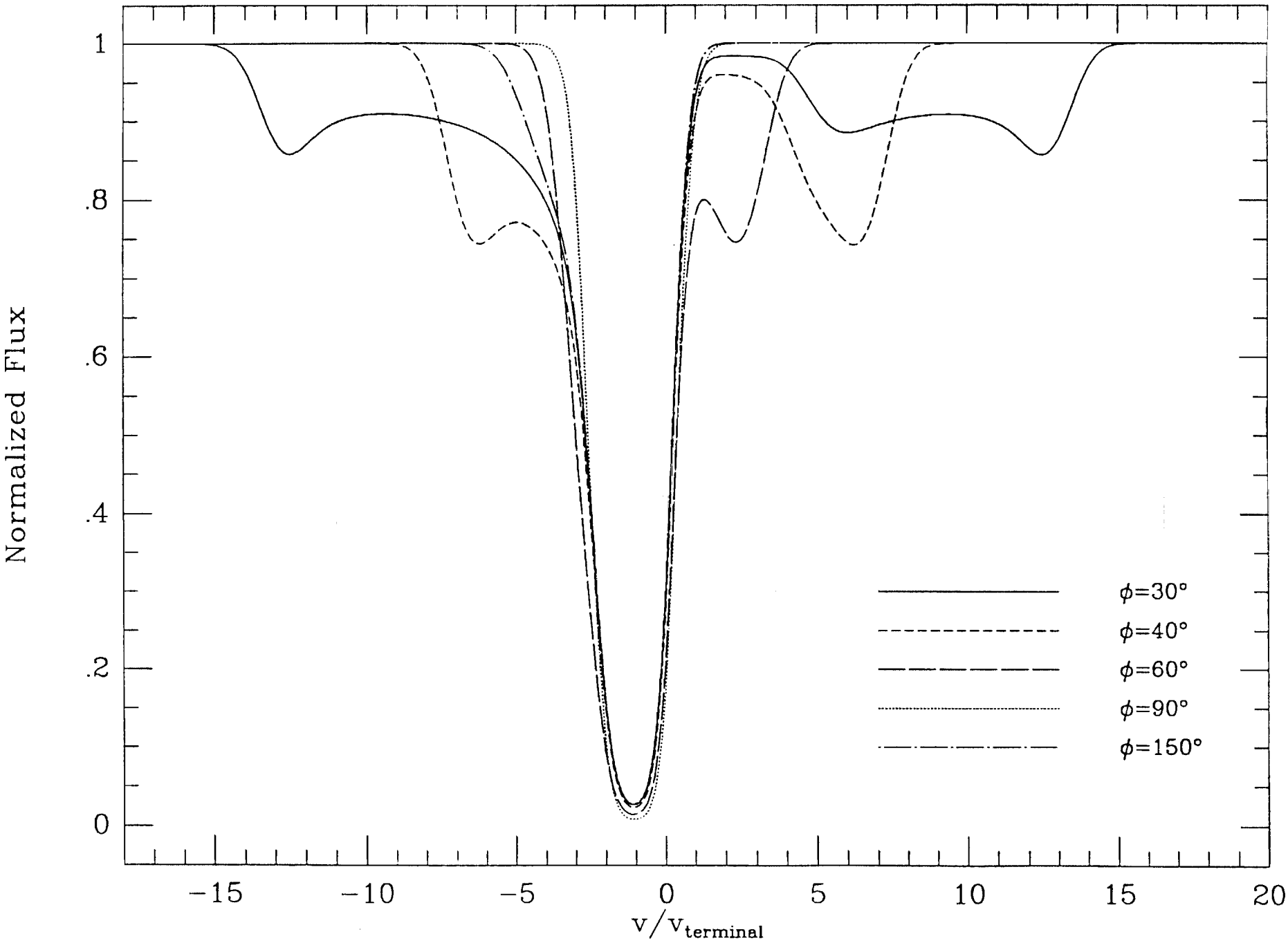
Normalized Flux
1
.8
.6
.4
.2
0
−15
−10
−5
0
5
10
15
20
v/v terminal
ϕ=30°
ϕ=40°
ϕ=60°
ϕ=90°
ϕ=150°

Fig 7.

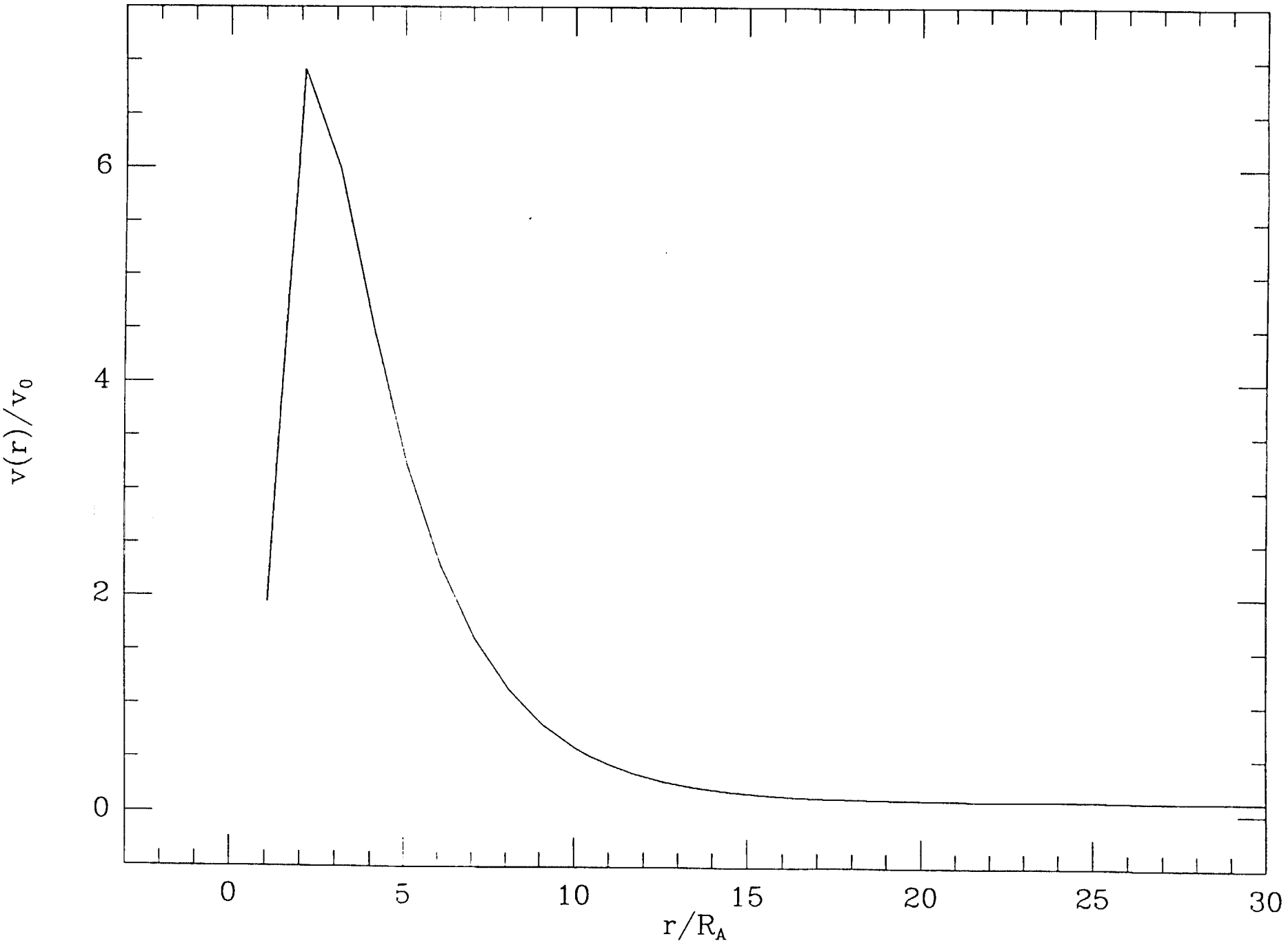
v(r)/v0
6
4
2
0
0
5
10
15
20
25
30
r/RA

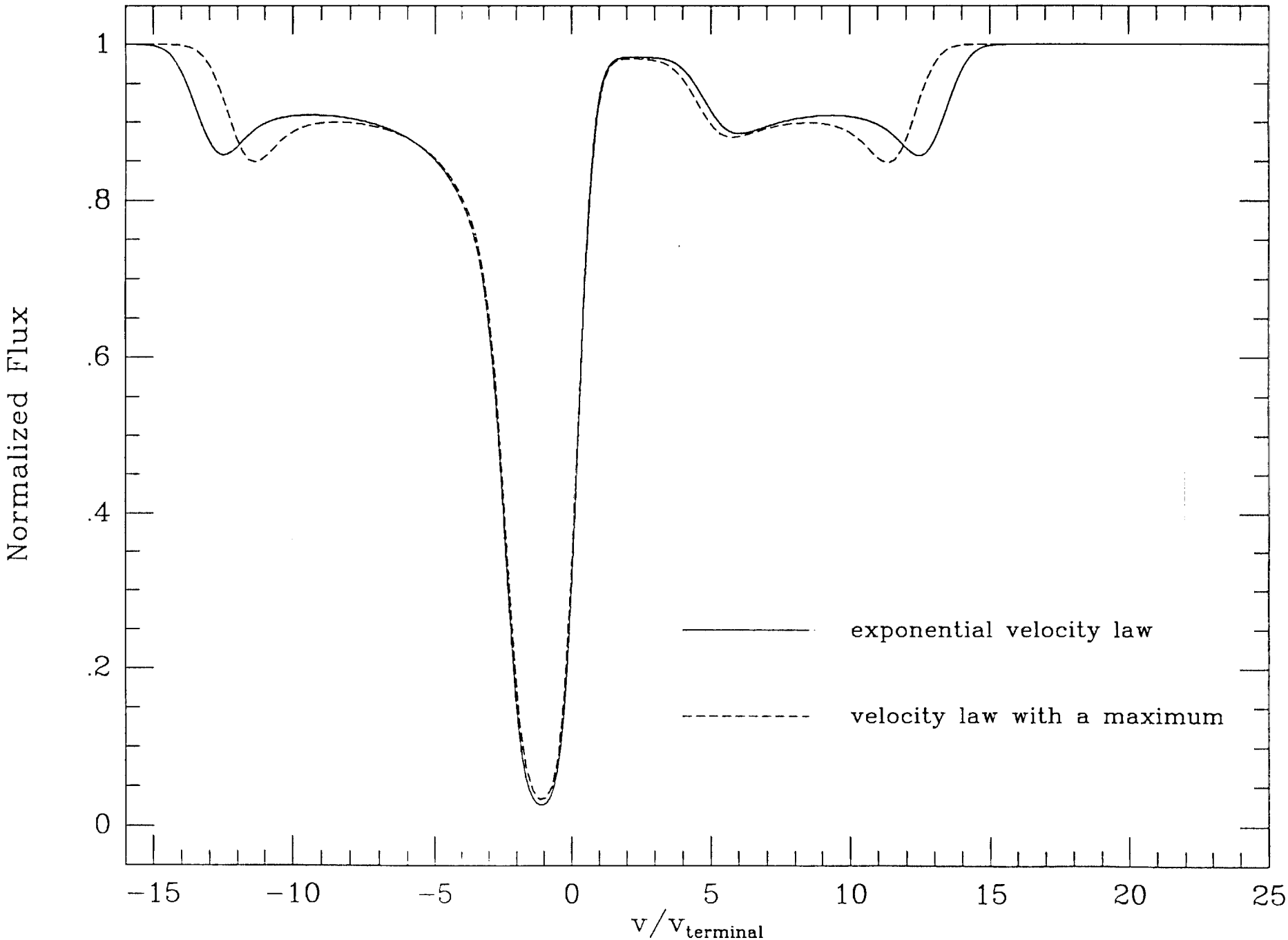
Normalized Flux
1
.8
.6
.4
.2
0
−15
−10
−5
0
5
10
15
20
25
V/V terminal
exponential velocity law
velocity law with a maximum

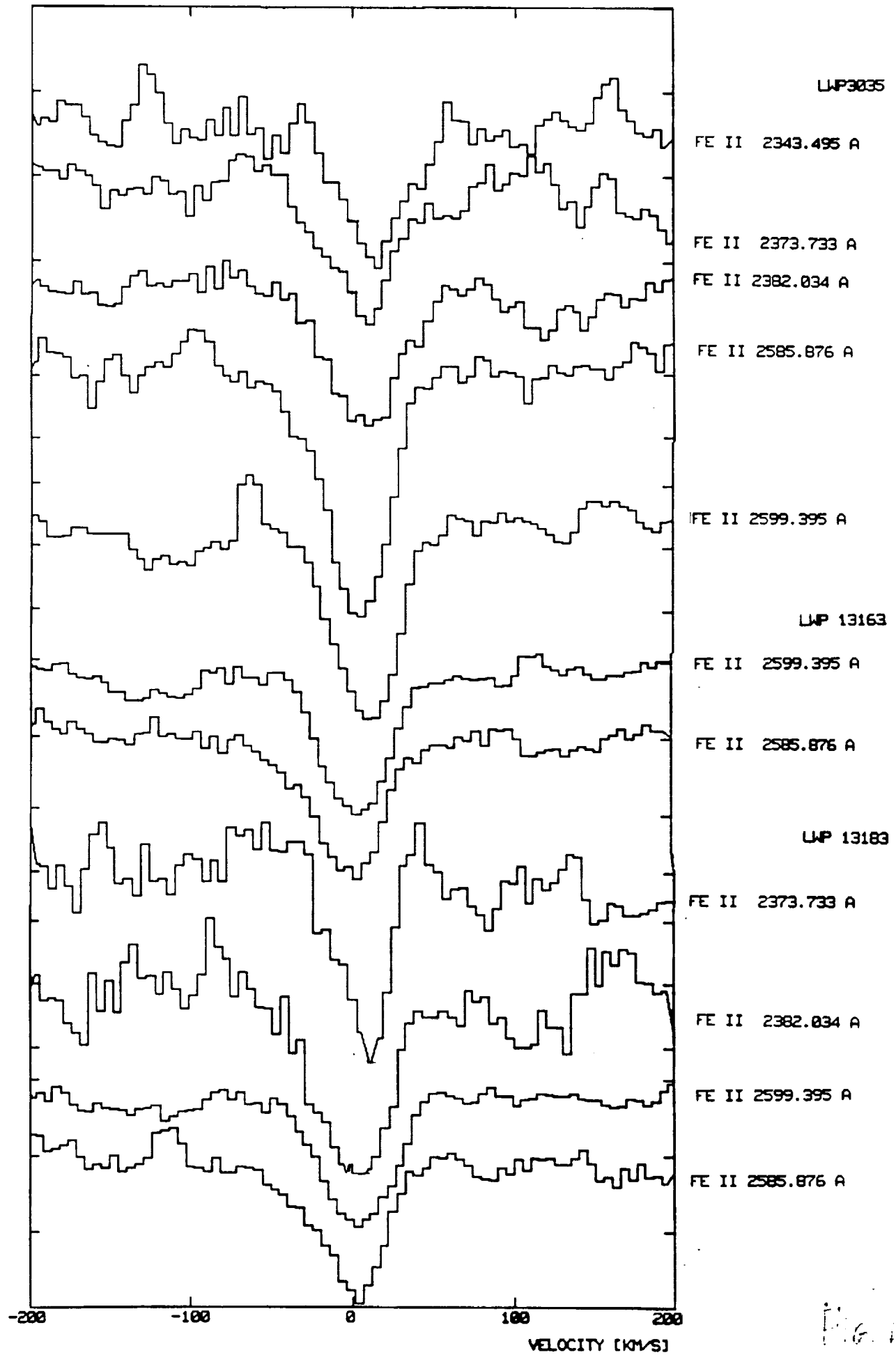
LWP3035
FE II 2343.495 A
FE II 2373.733 A
FE II 2382.034 A
FE II 2585.876 A
FE II 2599.395 A
LWP 13163
FE II 2599.395 A
FE II 2585.876 A
LWP 13183
FE II 2373.733 A
FE II 2382.034 A
FE II 2599.395 A
FE II 2585.876 A
-200
-100
0
100
200
VELOCITY [KM/S]

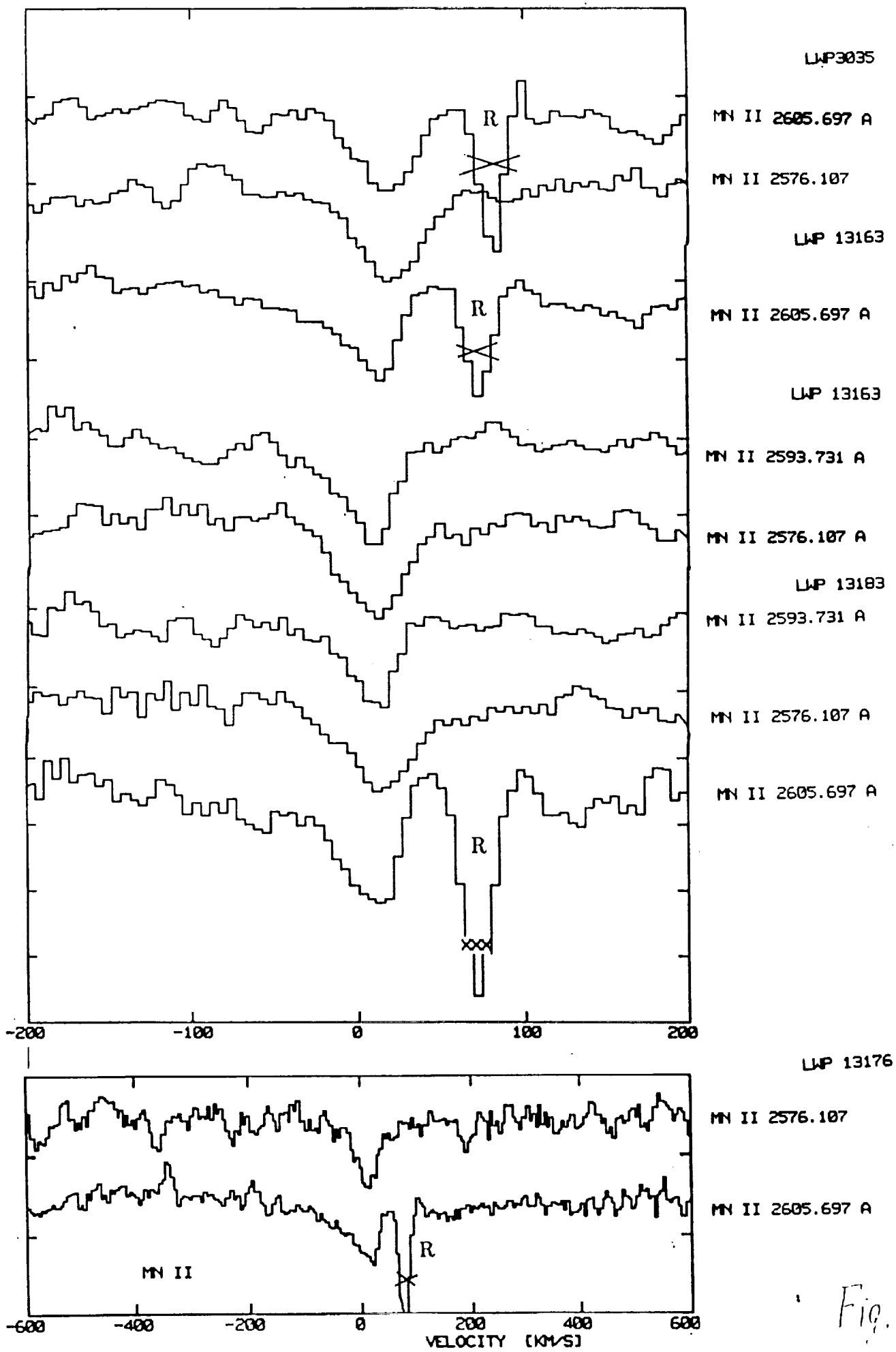
LWP3035
MN II 2605.697 A
MN II 2576.107
LWP 13163
MN II 2605.697 A
LWP 13163
MN II 2593.731 A
MN II 2576.107 A
LWP 13183
MN II 2593.731 A
MN II 2576.107 A
MN II 2605.697 A
R
-200
-100
0
100
200
LWP 13176
MN II 2576.107
MN II 2605.697 A
MN II
-600
-400
-200
0
200
400
600
VELOCITY (KM/S)

Fig. 11

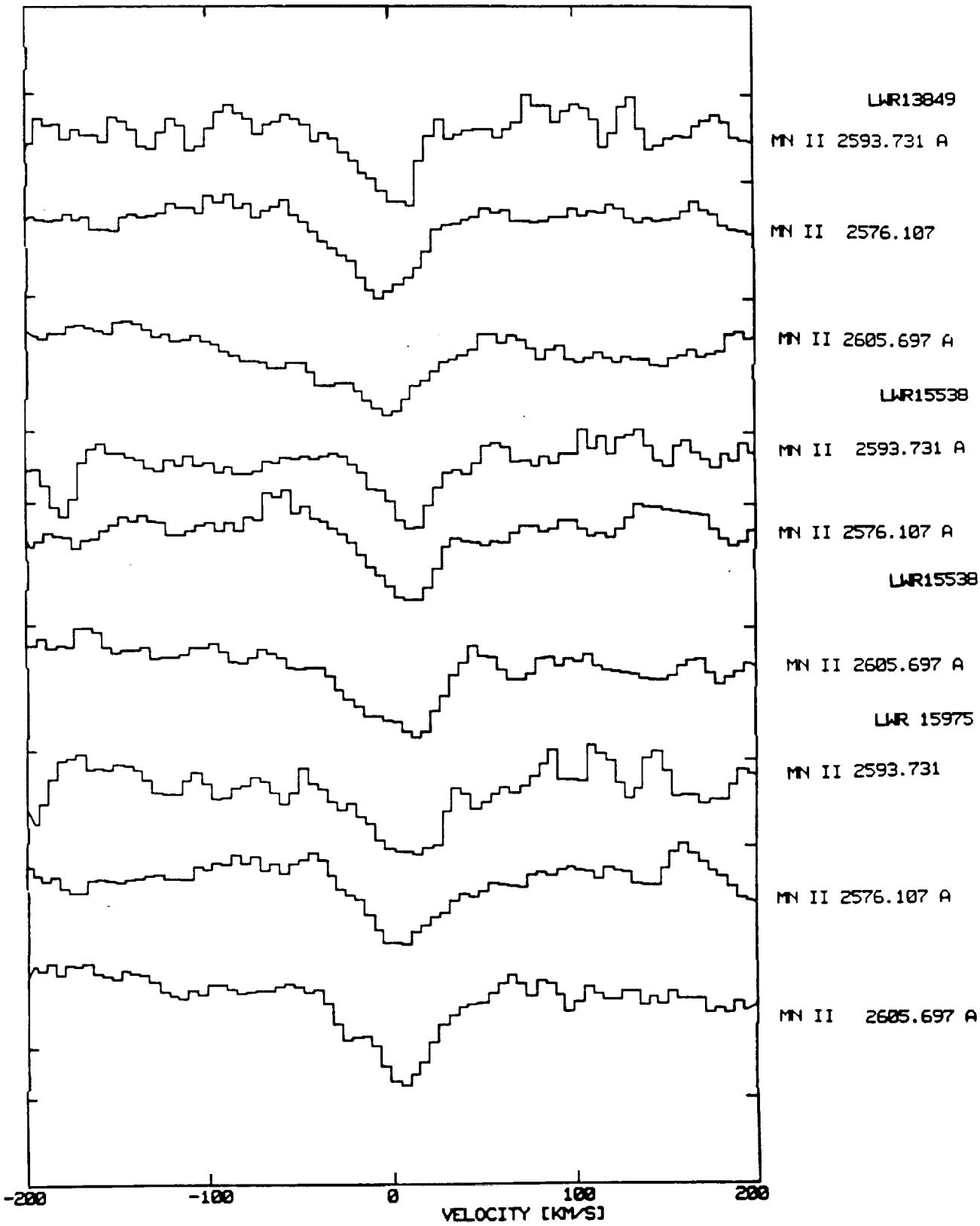

Cochinos & Bohannan, Fig 12

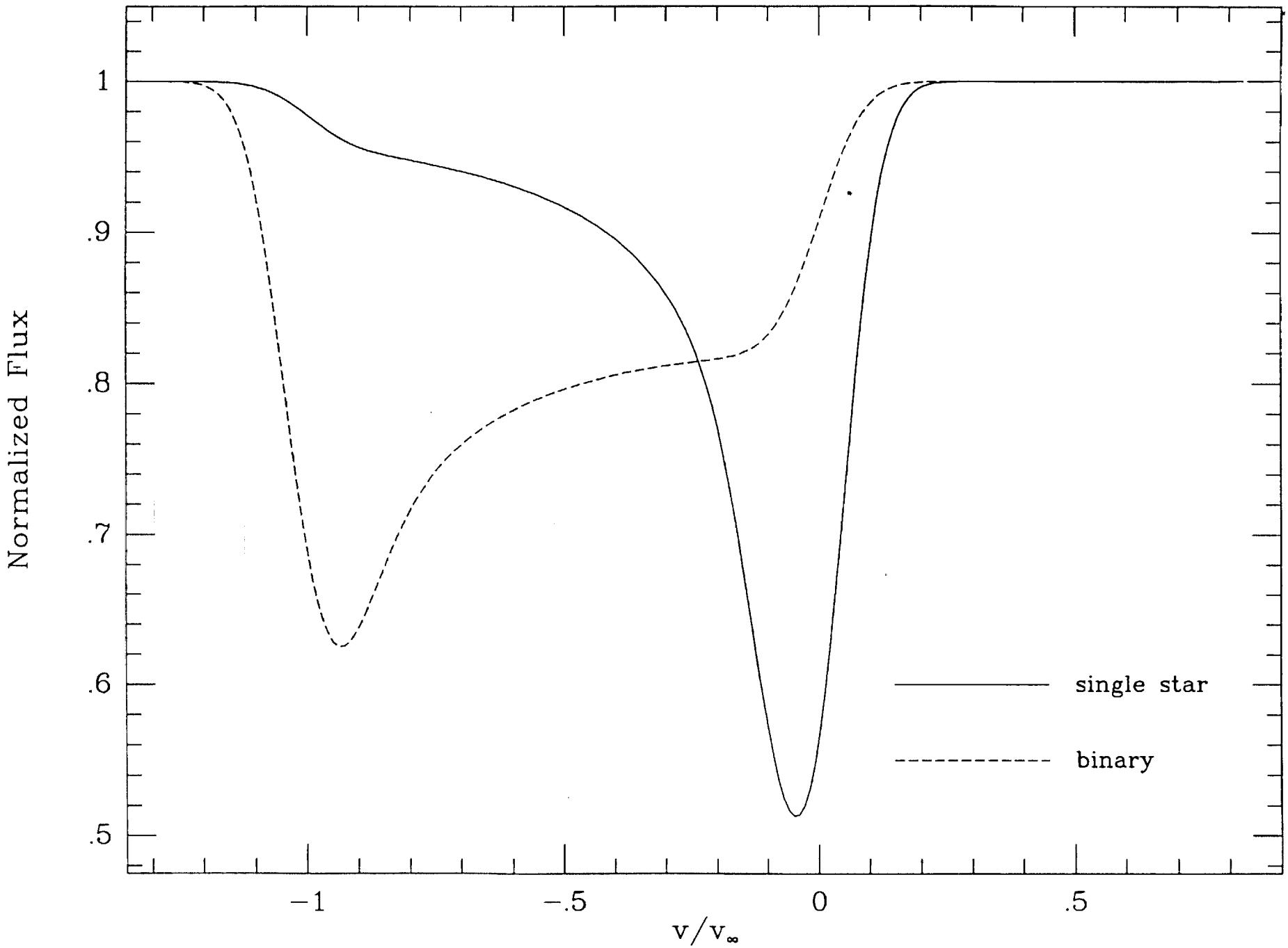
Normalized Flux
1
.9
.8
.7
.6
.5
−1
−.5
0
.5
v/v∞
single star
binary

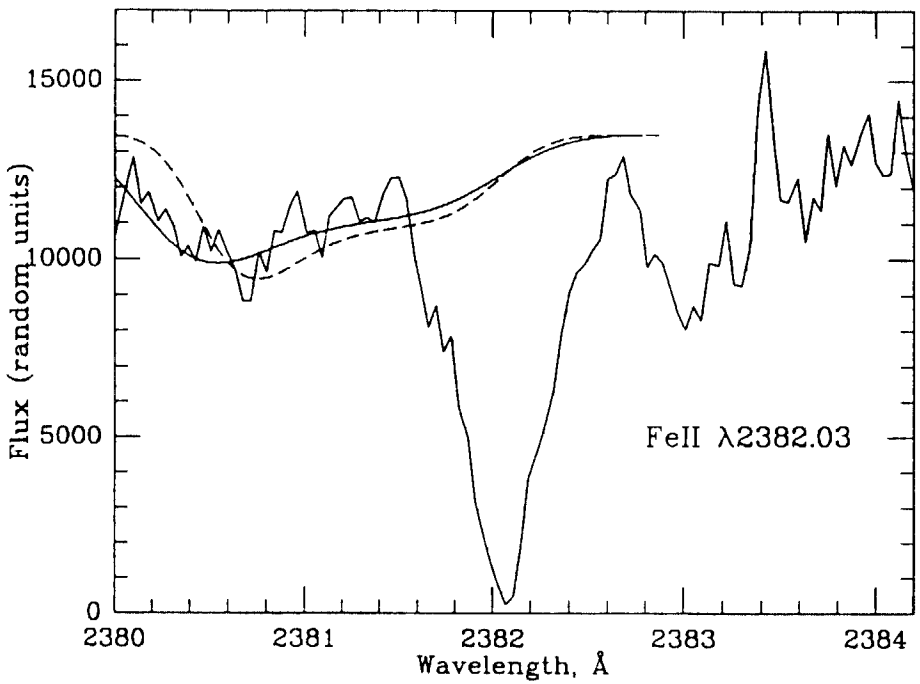
15000
10000
5000
0
Flux (random units)
FeII λ2382.03
2380
2381
2382
2383
2384
Wavelength, Å

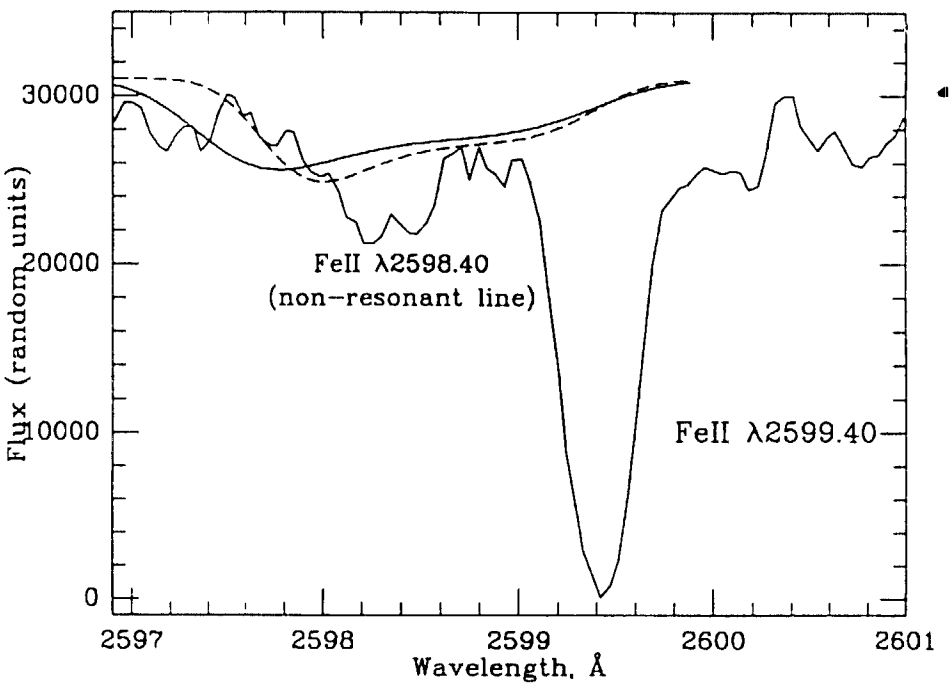
30000
20000
10000
0
Flux (random units)
FeII λ2598.40
(non-resonant line)
FeII λ2599.40
2597
2598
2599
2600
2601
Wavelength, Å

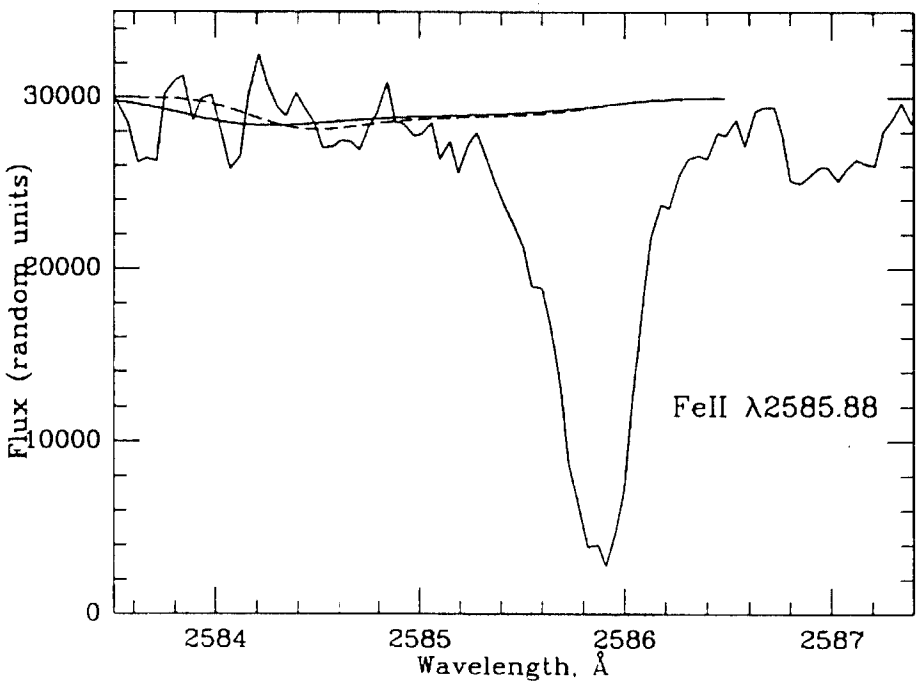
30000
20000
10000
0
Flux (random units)
FeII λ2585.88
2584
2585
2586
2587
Wavelength, Å

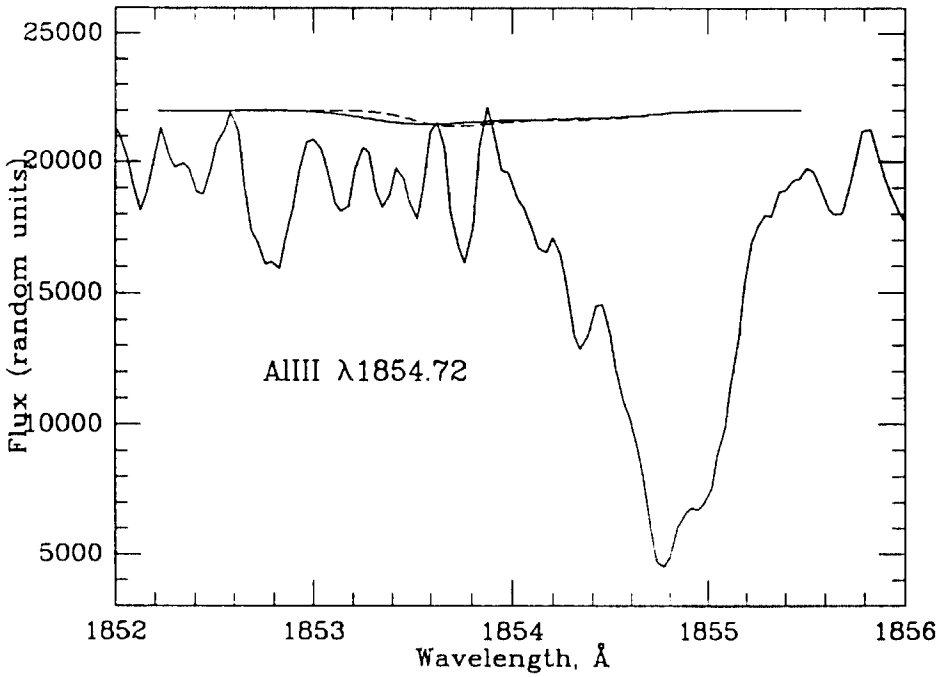
AlIII λ1854.72
Flux (random units)
Wavelength, Å
25000
20000
15000
10000
5000
1852
1853
1854
1855
1856

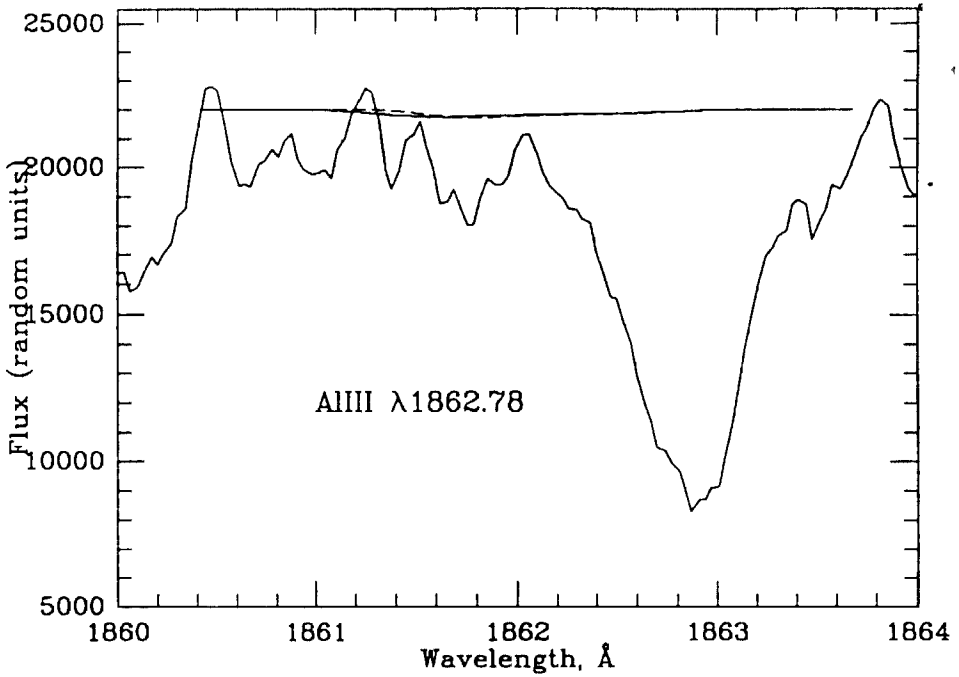
AlIII λ1862.78
Flux (random units)
Wavelength, Å
25000
20000
15000
10000
5000
1860
1861
1862
1863
1864

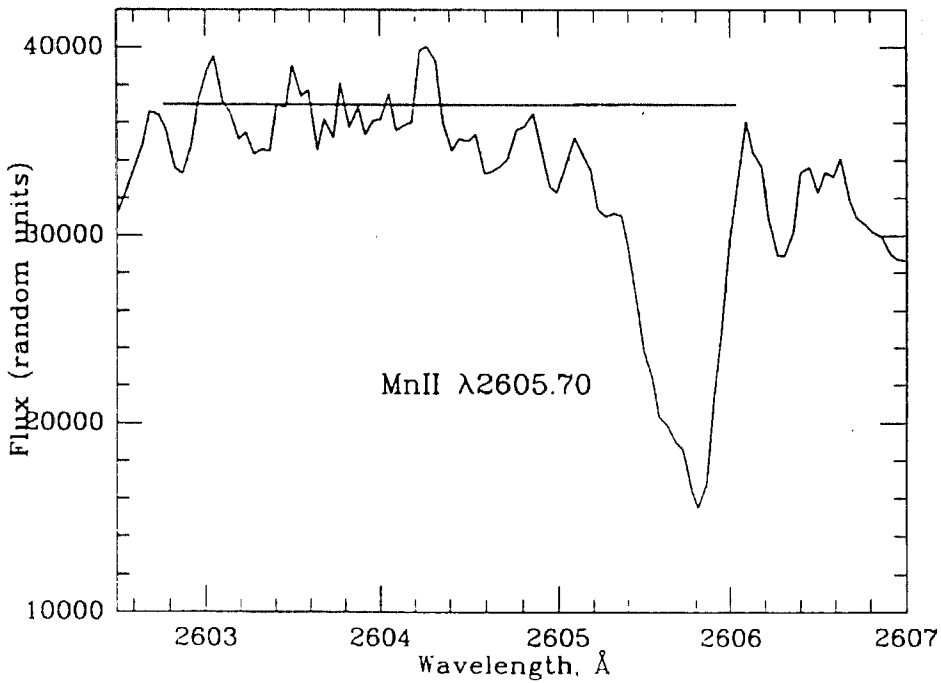
MnII λ2605.70
Flux (random units)
Wavelength, Å
40000
30000
20000
10000
2603
2604
2605
2606
2607

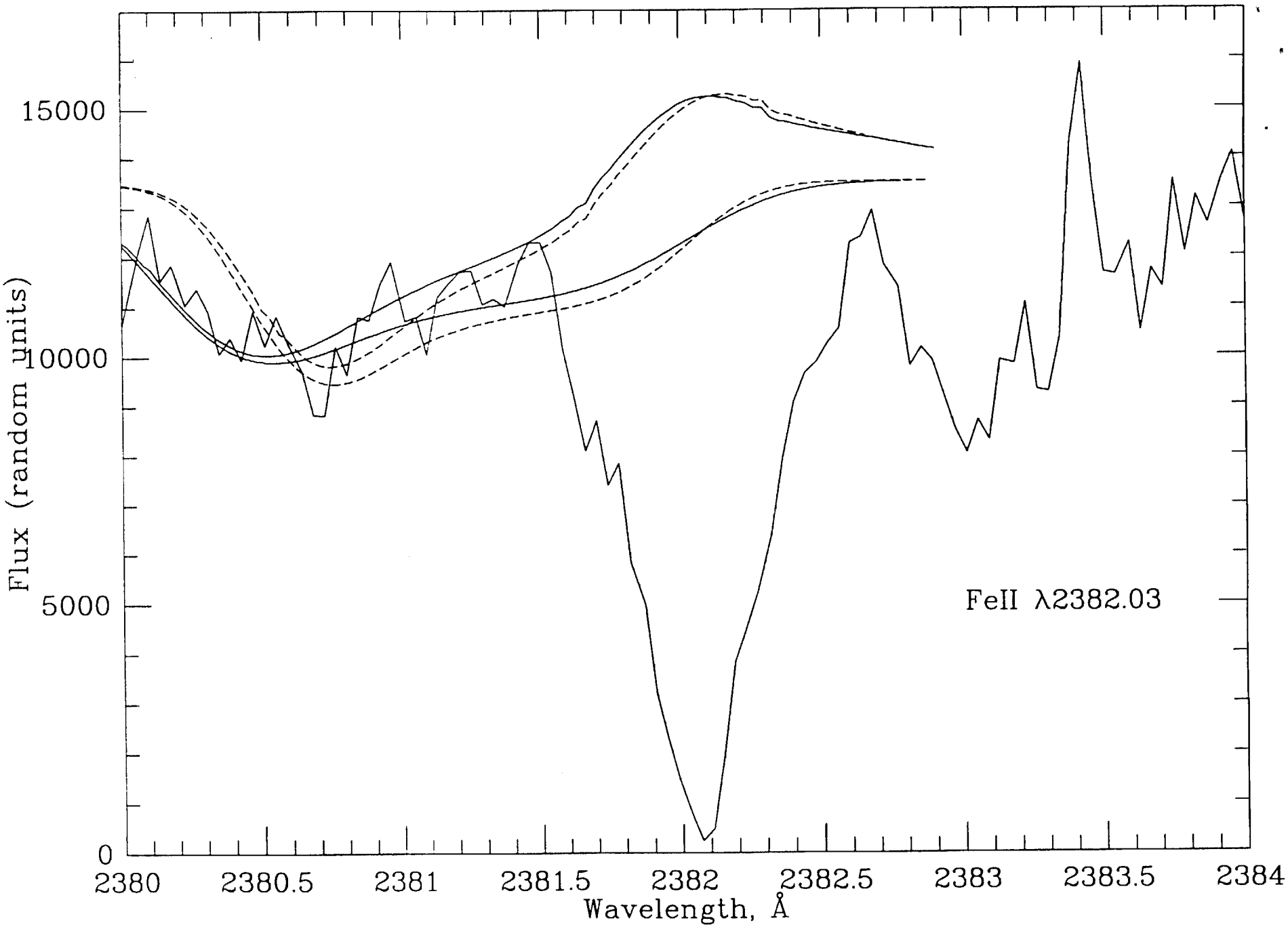
15000
10000
5000
0
Flux (random units)
2380
2380.5
2381
2381.5
2382
2382.5
2383
2383.5
2384
Wavelength, Å
FeII λ2382.03

Fig 15

AUTHORS' ADDRESSES:

ERIKA BÖHM-VITENSE

Astronomy Department, FM-20, University of Washington, Seattle, WA 98195

LILIYA L. RODRIGUES

Astronomy Department, FM-20, University of Washington, Seattle, WA 98195